

## THE X-RAY SPECTRAL PROPERTIES OF SCUBA GALAXIES

D.M. ALEXANDER,<sup>1</sup> F.E. BAUER,<sup>1</sup> S.C. CHAPMAN,<sup>2</sup> I. SMAIL,<sup>3</sup> A.W. BLAIN,<sup>2</sup> W.N. BRANDT,<sup>4</sup> AND R.J. IVISON<sup>5,6</sup>

<sup>1</sup>Institute of Astronomy, Madingley Road, Cambridge CB3 0HA, UK

<sup>2</sup>California Institute of Technology, Pasadena, CA 91125, USA

<sup>3</sup>Institute for Computational Cosmology, University of Durham, South Road, Durham DH1 3LE, UK

<sup>4</sup>Department of Astronomy and Astrophysics, Pennsylvania State University, 525 Davey Laboratory, University Park, PA 16802, USA

<sup>5</sup>Astronomy Technology Centre, Royal Observatory, Blackford Hill, Edinburgh EH9 3HJ, UK and

<sup>6</sup>Institute for Astronomy, University of Edinburgh, Blackford Hill, Edinburgh EH9 3HJ, UK

Received 2005 Feb 22; accepted 2005 June 23

### ABSTRACT

Deep SCUBA surveys have uncovered a large population of massive submillimeter emitting galaxies (SMGs;  $f_{850\mu\text{m}} \gtrsim 4$  mJy) at  $z \gtrsim 1$ . Although it is generally believed that these galaxies host intense star-formation activity, there is growing evidence that a substantial fraction also harbor an Active Galactic Nucleus [AGN; i.e., an accreting super-massive black hole (SMBH)]. We present here possibly the strongest evidence for this viewpoint to date: the combination of ultra-deep X-ray observations (the 2 Ms *Chandra* Deep Field-North) and deep Keck spectroscopic data of SMGs with radio counterparts. We find that the majority ( $\approx 75\%$ ) of these radio-selected spectroscopically identified SMGs host AGN activity; the other  $\approx 25\%$  have X-ray properties consistent with star formation (X-ray derived star-formation rates of  $\approx 1300\text{--}2700 M_{\odot}\text{yr}^{-1}$ ). The AGNs have properties generally consistent with those of nearby luminous AGNs ( $\Gamma \approx 1.8 \pm 0.5$ ,  $N_{\text{H}} \approx 10^{20}\text{--}10^{24} \text{ cm}^{-2}$ , and  $L_{\text{X}} \approx 10^{43}\text{--}10^{44.5} \text{ erg s}^{-1}$ ) and the majority ( $\approx 80\%$ ) are heavily obscured ( $N_{\text{H}} \gtrsim 10^{23} \text{ cm}^{-2}$ ). We construct composite rest-frame 2–20 keV spectra for three different obscuration classes ( $N_{\text{H}} < 10^{23} \text{ cm}^{-2}$ ,  $N_{\text{H}} = 1\text{--}5 \times 10^{23} \text{ cm}^{-2}$ , and  $N_{\text{H}} > 5 \times 10^{23} \text{ cm}^{-2}$ ) which reveal features not seen in the individual X-ray spectra. An  $\approx 1$  keV equivalent width Fe K $\alpha$  emission line is seen in the composite X-ray spectrum of the most heavily obscured AGNs, suggesting Compton-thick or near Compton-thick absorption. Even taking into account the effects of absorption, we find that the average X-ray to far-infrared luminosity ratio of the AGN-classified SMGs ( $\frac{L_{\text{X}}}{L_{\text{FIR}}} = 0.004$ ) is approximately one order of magnitude below that found for typical quasars. This result suggests that intense star-formation activity (of order  $\approx 1000 M_{\odot}\text{yr}^{-1}$ ) dominates the bolometric output of these SMGs. However, we also explore the possibility that the X-ray to far-infrared luminosity ratio of the AGN components is intrinsically less than that found for typical quasars and postulate that some SMGs may be AGN dominated. We investigate the implications of our results for the growth of massive black holes, discuss the prospects for deeper X-ray observations, and explore the scientific potential offered by the next generation of X-ray observatories.

*Subject headings:* infrared: galaxies — X-rays: galaxies — galaxies: active — galaxies: starburst

### 1. INTRODUCTION

Deep SCUBA surveys have uncovered a large population of submillimeter (submm;  $\lambda = 300\text{--}1000 \mu\text{m}$ ) emitting galaxies (SMGs;  $\lesssim 1000$  sources  $\text{deg}^{-2}$  at  $f_{850\mu\text{m}} \gtrsim 4$  mJy; e.g., Smail, Ivison, & Blain 1997; Barger, Cowie & Sanders 1999; Blain et al. 1999, 2002; Eales et al. 1999; Cowie et al. 2002; Scott et al. 2002; Borys et al. 2003; Webb et al. 2003a). The majority of these SMGs are faint at all other wavelengths, hindering source identification studies (e.g., Hughes et al. 1998; Ivison et al. 2000; Smail et al. 2002; Webb et al. 2003b). However, due to a considerable amount of intensive multi-wavelength follow-up effort, it is becoming clear that almost all are dust-enshrouded luminous galaxies at  $z > 1$  (e.g., Ivison et al. 1998, 2000; Barger et al. 1999; Chapman et al. 2003a, 2005; Simpson et al. 2004; Pope et al. 2005). With estimated bolometric luminosities of order  $10^{13} L_{\odot}$  (Blain et al. 2004a; Chapman et al. 2005), SMGs outnumber comparably luminous galaxies in the local Universe by several orders of magnitude (e.g., Cowie et al. 2004). Dynamical mass and galaxy clustering studies of spectroscopically identified SMGs have indicated that they are likely to be massive galaxies (e.g., Frayer et al. 1998, 1999; Genzel et al. 2003; Neri et al. 2003; Blain et al. 2004b; Swin-

bank et al. 2004; Greve et al. 2005); these SMGs are  $\approx 5$  times more massive than the coeval optically selected field galaxies (e.g., Erb et al. 2003; Steidel et al. 2004; Swinbank et al. 2004). Making reasonable assumptions about the duration of the submm-bright phase in these systems, these results provide evidence that SMGs are the progenitors of local  $\gtrsim M_{*}$  early-type galaxies (e.g., Lilly et al. 1999; Scott et al. 2002; Smail et al. 2004; Chapman et al. 2005).

Central to the study of SMGs is the physical origin of their extreme luminosities [i.e., starburst or Active Galactic Nucleus (AGN) activity]. If these sources are shown to be ultra-luminous starburst galaxies then their derived star-formation rates suggest a substantial increase in star-formation activity at  $z > 1$  (e.g., Blain et al. 1999; Smail et al. 2002). Conversely, if these sources are shown to be powerful AGNs then they outnumber comparably luminous optical quasars by  $\approx 1\text{--}2$  orders of magnitude. The apparent association of a few SMGs with quasars and their comparable comoving space densities (when corrected for probable source lifetimes) suggest an evolutionary connection between these two populations (e.g., Page et al. 2001, 2004; Croom et al. 2004; Stevens et al. 2003, 2004; Chapman et al. 2005). Given this evidence it is plausible that SMGs represent a rapid black-hole and stellar growth stage prior to a luminous quasar phase (e.g., Archibald et al. 2002;

Almaini 2003; Page et al. 2004; Alexander et al. 2005a).

Arguably the most direct indication of AGN activity is the detection of luminous hard X-ray emission (i.e.,  $> 2$  keV). Hard X-ray emission appears to be a universal property of AGNs, giving a direct “window” on the emission regions closest to the SMBH (e.g., Mushotzky, Done, & Pounds 1993), and it can provide a secure AGN identification in sources where the optical signatures and counterparts are weak or even non-existent (e.g., Alexander et al. 2001; Comastri et al. 2002). Hard X-ray emission is relatively insensitive to obscuration (at least for sources that are Compton thin; i.e.,  $N_{\text{H}} \lesssim 1.5 \times 10^{24} \text{ cm}^{-2}$ ) and any hard X-ray emission from star formation in the host galaxy is often insignificant when compared to that produced by the AGN.

The first cross-correlation studies of moderately deep ( $\approx 20$ – $200$  ks) *Chandra* surveys with SCUBA surveys yielded little overlap between the X-ray and submm detected source populations ( $\lesssim 10$ – $20\%$ ; e.g., Fabian et al. 2000; Bautz et al. 2000; Hornschemeier et al. 2000; Severgnini et al. 2000).<sup>1</sup> To first order these results suggested that bolometrically dominant AGNs can only be present in typical SMGs if they are Compton thick. Later studies with the *Chandra* Deep Field-North (CDF-N; Brandt et al. 2001, Alexander et al. 2003a) survey showed that a significant fraction (upwards of  $\approx 30$ – $50\%$  when the Borys et al. 2003 SCUBA map is used) of SMGs are X-ray detected (Barger et al. 2001b; Alexander et al. 2003b; Borys et al. 2004). Direct X-ray spectral analyses of the five AGN-classified SMGs in Alexander et al. (2003b) indicated that the AGNs were heavily obscured but only moderately luminous at X-ray energies ( $L_{\text{X}} \approx 0.3$ – $1 \times 10^{44} \text{ erg s}^{-1}$  when corrected for the effects of absorption). A comparison of the X-ray-to-submm spectral slopes of these SMGs to that of NGC 6240 (a nearby luminous galaxy with an obscured AGN) suggested that the AGNs typically contributed only a few percent of the bolometric luminosity. However, the small sample size and lack of spectroscopic redshifts (only one source had a spectroscopic redshift) prevented more quantitative conclusions.

The deep optical spectroscopic work of Chapman et al. (2003a, 2005) has recently provided spectroscopic redshifts for 73 radio-identified SMGs, a significant increase in sample size over previous studies (e.g., Ivison et al. 1998, 2000; Barger et al. 1999; Ledlow et al. 2002; Smail et al. 2003; Simpson et al. 2004). The 2 Ms CDF-N field was one of the regions targeted for this intensive spectroscopic follow up. The combination of deep optical spectroscopic data and ultra-deep X-ray observations provides powerful constraints on AGNs in SMGs. In particular, spectroscopic redshifts improve the accuracy of the X-ray spectral analyses over those of Alexander et al. (2003b) through the identification of discrete X-ray spectral features (e.g., Fe K $\alpha$  emission) and the determination of any intrinsic absorption, which is a strong function of redshift in a given X-ray band [ $N_{\text{H},z} \approx N_{\text{H},z0}(1+z)^{2.6}$ ]. These improvements promise the most accurate determination of the AGN contribution to the bolometric output of these SMGs to date. In this paper we investigate the X-ray properties of the radio-selected spectroscopically identified SMGs in the CDF-N field and predict the AGN contribution to the bolometric luminosity of these SMGs. The Galactic column

density toward the CDF-N field is  $(1.3 \pm 0.4) \times 10^{20} \text{ cm}^{-2}$  (Lockman 2004), and  $H_0 = 65 \text{ km s}^{-1} \text{ Mpc}^{-1}$ ,  $\Omega_{\text{M}} = \frac{1}{3}$ , and  $\Omega_{\Lambda} = \frac{2}{3}$  are adopted throughout.

## 2. OBSERVATIONS AND BASIC ANALYSIS

### 2.1. SCUBA Galaxy Sample

Our SCUBA galaxy sample includes 20 SMGs that have been spectroscopically identified by Chapman et al. (2005) and lie in the region of the 2 Ms CDF-N observation (Alexander et al. 2003a). The optical counterparts for these sources were chosen based on the positional association with a radio source [identified by either VLA (Richards 2000) or MERLIN (Chapman et al. 2004a) observations]. The basic properties of the SMGs are given in Table 1. The source redshifts ( $z = 0.555$ – $2.914$  with a median of  $z = 2.0 \pm 0.6$ ) are typical of the spectroscopically identified SMG population (median redshift of  $z \approx 2.2$ ; Chapman et al. 2005). The  $\approx 35$ – $50\%$  of sources without radio counterparts (e.g., Ivison et al. 2002; Chapman et al. 2003b; Borys et al. 2004) could not be targeted with optical spectroscopy. However, the range of  $850\mu\text{m}$  flux densities for the submm sample ( $f_{850\mu\text{m}} \approx 4$ – $12$  mJy, with a mean of  $6.6 \pm 2.2$  mJy) is typical of SMGs detected in blank-field SCUBA surveys (e.g., Scott et al. 2002; Webb et al. 2003a).

The potential selection effects introduced by the radio and spectroscopic-identification of this sample, compared to a purely submm-flux-limited sample of SMGs, are discussed at length in Chapman et al. (2005) and Blain et al. (2004). The need for both a faint radio counterpart and identifiable spectral features to aid in redshift measurement may result in this sample having a higher incidence of AGN activity than the SMG population as a whole; however, the incompleteness in our surveys due to these two selection criteria can be equally well explained by the likely temperature and redshift distribution of the SMG population (Chapman et al. 2005). Nevertheless, we caution the reader that the sample analysed here may not be completely representative of the entire  $f_{850\mu\text{m}} \gtrsim 4$  mJy SMG population.

Many of the SMGs in our sample were radio-selected sources specifically targeted with SCUBA observations; see the table in Alexander et al. (2005a) for the observation modes. While this could potentially cause an additional AGN bias over a purely radio-detected SMG sample, we do not find evidence for a strong bias in our sample (see Alexander et al. 2005a for the results of a two-sided Fisher’s exact test).

### 2.2. *Chandra* Counterparts to the SCUBA Galaxy Sample

The 2 Ms CDF-N observations were centered on the optical Hubble Deep Field-North (HDF-N; Williams et al. 1996) region and cover  $\approx 448 \text{ arcmin}^2$  (Alexander et al. 2003a). These observations provide the deepest view of the Universe in the 0.5–8.0 keV band; the aim-point sensitivities are  $\approx 7.1 \times 10^{-17} \text{ erg cm}^{-2} \text{ s}^{-1}$  at 0.5–8.0 keV (full band),  $\approx 2.5 \times 10^{-17} \text{ erg cm}^{-2} \text{ s}^{-1}$  at 0.5–2.0 keV (soft band), and  $\approx 1.4 \times 10^{-16} \text{ erg cm}^{-2} \text{ s}^{-1}$  at 2–8 keV (hard band). At the median redshift of the SMGs, the observed 0.5–8.0 keV band corresponds to rest-frame energies of 1.5–24 keV. Such high X-ray energies allow very high column densities to be penetrated (e.g., at 20 keV,  $\lesssim 55\%$  of the direct X-ray emission

<sup>1</sup> Further cross-correlation studies with moderately deep X-ray observations have revealed some overlap (e.g., Barger et al. 2001a; Ivison et al. 2002; Almaini et al. 2003; Waskett et al. 2003). This was probably due to the larger areal coverage of the SCUBA observations in these studies.

is absorbed with column densities of  $N_{\text{H}} \lesssim 10^{24} \text{ cm}^{-2}$ ; see Appendix B in Deluit & Courvoisier 2003).

Using a  $1.5''$  search radius, 16 of the 20 SMGs were found to have *Chandra* counterparts in the main *Chandra* catalog of Alexander et al. (2003a). Given the low surface density of SMGs, we also searched for X-ray counterparts using the complete supplementary *Chandra* catalog of Alexander et al. (2003a) and found one further match; the probability of this match being spurious is  $< 1\%$  (see §2.4 of Alexander et al. 2003b). In total 17 ( $85^{+15}_{-20}\%$ ) of the 20 SMGs in our sample have a *Chandra* counterpart (see Table 1).<sup>2</sup> We have calculated rest-frame 0.5–8.0 keV luminosities, and 1.4 GHz luminosity densities following equations 1 and 2 in Alexander et al. (2003b), assuming an X-ray spectral slope of  $\Gamma = 1.8$  and a radio spectral slope of  $\alpha = 0.8$ , respectively. Far-infrared (far-IR;  $\lambda = 40\text{--}120 \mu\text{m}$ ) luminosities were calculated from the rest-frame 1.4 GHz luminosity densities under the assumption of the radio-to-far-IR correlation with  $q = 2.35$  (e.g., Helou, Soifer, & Rowan-Robinson 1985); the presence of an AGN component to the radio emission will lead to an overprediction of the far-IR luminosity. See Table 1.

The three X-ray undetected SMGs lie in sensitive regions of the CDF-N field and have  $3 \sigma$  flux limits below the fluxes of the X-ray detected SMGs; see Table 1. Their redshifts ( $z = 2.0\text{--}2.1$ ) are consistent with the median redshift of the SMG sample. Stacking the X-ray data of the individually undetected SMGs following the procedure of Lehmer et al. (2005) yields marginally significant detections in the soft and full bands ( $2.5\sigma$ , soft band;  $2.7\sigma$ , full band; S. Immler, private communication), suggesting that these sources lie just below the individual source detection limit. The corresponding average X-ray constraints are  $\approx 9.0 \times 10^{-17} \text{ erg cm}^{-2} \text{ s}^{-1}$  (full band),  $\approx 1.7 \times 10^{-17} \text{ erg cm}^{-2} \text{ s}^{-1}$  (soft band) and  $< 1.6 \times 10^{-16} \text{ erg cm}^{-2} \text{ s}^{-1}$  (hard band). The full-band constraint corresponds to  $L_{0.5\text{--}8.0 \text{ keV}} \approx 2 \times 10^{42} \text{ erg s}^{-1}$  at  $z = 2$  for  $\Gamma = 1.8$  and is consistent with that expected from luminous star formation (see §3.2 and §4.2).

### 2.3. X-ray Spectra: Extraction and Fitting

X-ray spectra were generated for all of the SMGs with full-band fluxes  $> 3 \times 10^{-16} \text{ erg cm}^{-2} \text{ s}^{-1}$ , which typically corresponds to  $> 50$  X-ray counts. To account for the range of roll angles and aim points in the 20 separate observations that comprise the 2 Ms CDF-N, the X-ray spectra were generated using the ACIS source extraction code (ACIS EXTRACT) described in Broos et al. (2002).<sup>3</sup> Briefly, for each source this code extracts the counts from each of the observations taking into account the changing shape and size of the PSF with off-axis angle as given in the *Chandra* X-ray Center (CXC) PSF library.<sup>4</sup> A local background is extracted after all of the sources are excluded from the X-ray event file, and the spectra and response matrices are summed using standard FTOOLS routines (Blackburn 1995). See F. E. Bauer et al. (in preparation) for further information and the X-ray spectral properties of the sources detected in the *Chandra* deep fields.

Given the limited counting statistics of the X-ray sources, we performed all of the X-ray spectral analyses using the *C*-statistic (Cash 1979). One advantage of using the *C*-statistic

<sup>2</sup> All errors are taken from Tables 1 and 2 of Gehrels (1986) and correspond to the  $1\sigma$  level; these were calculated assuming Poisson statistics.

<sup>3</sup> ACIS EXTRACT is a part of the TARA software package and can be accessed from [http://www.astro.psu.edu/xray/docs/TARA/ae\\_users\\_guide.html](http://www.astro.psu.edu/xray/docs/TARA/ae_users_guide.html).

<sup>4</sup> See [http://asc.harvard.edu/ciao2.2/documents\\_dictionary.html#psf](http://asc.harvard.edu/ciao2.2/documents_dictionary.html#psf).

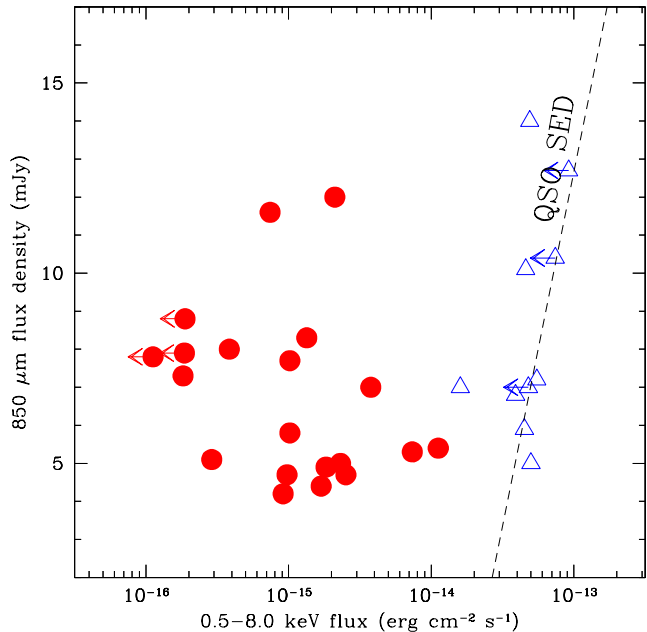


FIG. 1.— Submm flux density versus full-band flux for the SMGs (filled circles) and optically classified quasars with X-ray and submm constraints (open triangles). The quasar data are taken from Page et al. (2001), Vignali et al. (2001), and Isaak et al. (2002). The dashed line indicates the expected X-ray fluxes and submm flux densities for a quasar with the same properties as 3C273; the submm-to-X-ray spectral slope is independent of redshift (see Figure 2 of Fabian et al. 2000). Our spectroscopically identified SMGs are up to two orders of magnitude fainter in the X-ray band than the optically classified quasars for a given submm flux density.

is that the data can be fitted without binning, making it ideally suited to low-count sources (e.g., Nousek & Shue 1989). A disadvantage of using the *C*-statistic is that it is not possible to determine rigorously if one model provides a statistically preferable fit than another; however, it is possible to inspect the fit residuals and perform Monte-Carlo analyses to distinguish between different models. Hence in our analyses we have focused on empirically motivated models which have proven to provide a robust characterisation of the properties of well-studied AGNs. We used the latest version of XSPEC (v11.3.1; Arnaud 1996, 2002) for all of the model fitting, which allows the *C*-statistic to be used on background-subtracted data; we carried out several checks of the background-subtraction method to verify that no spurious residual features were present in the background-subtracted data. We fitted the X-ray spectra of the SMGs using a power law model (with Galactic absorption) in the rest-frame 2–10 keV and 5–20 keV bands; see Table 2. The constraints on the five sources with  $\lesssim 100$  counts are poor. However, our analyses have been designed to maximize the useful constraints for even the weakest X-ray sources. The fit parameter uncertainties are quoted at the 90% confidence level for one parameter of interest (Avni 1976). We provide details of our analysis techniques below but defer the discussion of our results to §3.

In order to interpret the X-ray spectral fitting results we have developed an empirically motivated AGN model and constructed a simple rest-frame power-law diagnostic diagram. The advantage of this approach is that we only need to perform simple rest-frame power law fits to the sources, allowing us to determine the characteristics of sources with few

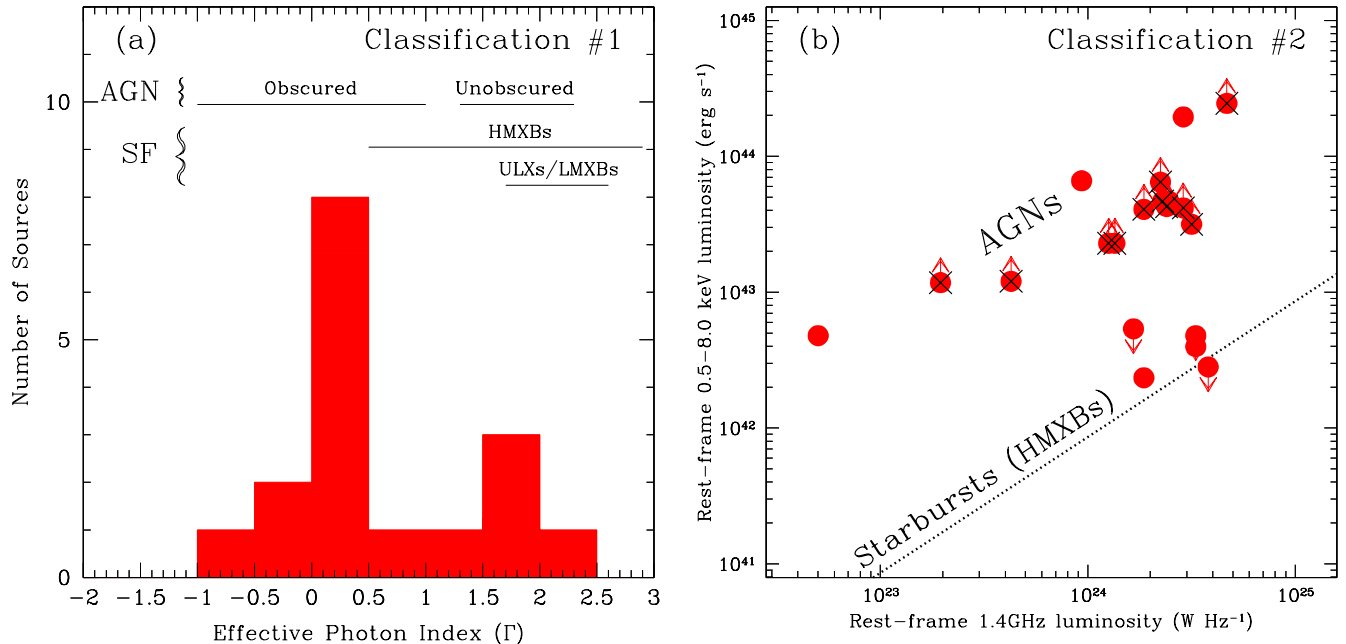


FIG. 2.—Classification scheme for the X-ray emission from the SMGs. (a) Effective photon-index histogram. The approximate observed X-ray spectral slopes for a variety of different source types [split broadly into AGN and star formation (SF)] are shown (e.g., Nandra & Pounds 1994; Maiolino et al. 1998; Colbert et al. 2004). The only sources that produce extremely flat or inverted X-ray spectral slopes ( $\Gamma < 0.5$ ) are obscured AGNs. The typical uncertainties in the X-ray spectral slopes for the plotted sources are  $\Delta\Gamma \approx 0.3$ ; see Table 1. (b) Rest-frame 0.5–8.0 keV luminosity versus 1.4 GHz luminosity density. The sources classified as obscured AGNs from Figure 2a are indicated with crosses; the X-ray luminosities have not been corrected for the effect of absorption. The dotted line shows the X-ray–radio relationship for star-forming galaxies whose X-ray emission is dominated by HMXBs (Persic et al. 2004); this relationship is converted to the 0.5–8.0 keV band from the 2–10 keV band assuming  $\Gamma = 1.8$ . The X-ray emission from 15 ( $\approx 75\%$ ) of the 20 SMGs is dominated by AGN activity. We caution the reader that due to selection biases this does not directly indicate a  $\approx 75\%$  AGN fraction in the bright SMG population; see §3.2.

X-ray counts. Our adopted AGN model includes a power-law component (which can be absorbed by neutral material;  $N_{\text{H}}$ ), a neutral reflection component (the PEXRAV model in XSPEC), a scattered component (Sc) of ionised gas, and a Fe  $K\alpha$  emission line at 6.4 keV. The XPSEC model components for our adopted model are (POW+PEXRAV+ZGA)+POW\*ZWABS.

We used the XSPEC command *fakeit* to produce the model tracks for a range of X-ray spectral slopes ( $\Gamma = 1.3$ – $2.3$ ) and absorbing column densities ( $N_{\text{H}} = 10^{20}$ – $2 \times 10^{24}$   $\text{cm}^{-2}$ ). The ratio of the direct to reflected emission (i.e., *rel\_refl* in the PEXRAV model) was fixed to unity, in agreement with the average value found for local AGNs (e.g., Risaliti et al. 2002; Deluit & Courvoisier 2003; Malizia et al. 2003). We set the other parameters of the neutral reflection component to be the same as those in Model 2c of Malizia et al. (2003). The ionised gas scattering fraction was set to be 1% of the intrinsic power-law emission, and the equivalent width of the Fe  $K\alpha$  emission line was varied depending on the absorbing column density ( $W_{\lambda} = 0.145$  keV for  $N_{\text{H}} < 3 \times 10^{23}$   $\text{cm}^{-2}$ ,  $W_{\lambda} = 0.37$  keV for  $N_{\text{H}} = 3$ – $7 \times 10^{23}$   $\text{cm}^{-2}$ , and  $W_{\lambda} = 1.0$  keV for  $N_{\text{H}} > 7 \times 10^{23}$   $\text{cm}^{-2}$ ; see Risaliti 2002 and Malizia et al. 2003). We also investigated higher column densities with a varying amount of ionised gas scattering fraction [ $N_{\text{H}} \approx 10^{25}$   $\text{cm}^{-2}$  (i.e., pure reflection) and Sc = 0–10%]. To take account of the *Chandra* ACIS-I instrumental response we used the response matrix file (RMF) and ancillary response file (ARF) from CXOHDFN J123629.1+621045. To allow for the construction of the model tracks up to rest-frame energies of 20 keV we assumed a redshift of  $z = 2.0$ , consistent with the average redshift of the SMG sample.

We also attempted to fit directly the individual X-ray spectra of the SMGs with the empirically motivated model outlined above. However, we could not statistically constrain these models sufficiently to gain additional physical insight over that found using the power-law diagnostic diagram analyses. This was most likely due to a degeneracy in the number of model components and the generally poor photon statistics of the individual X-ray spectra.

### 3. X-RAY PROPERTIES OF THE SCUBA GALAXY SAMPLE

#### 3.1. Basic Source Properties

We show the submm flux density versus full-band flux of all of the SMGs in Figure 1. As a comparison we also show the submm and X-ray properties of samples of moderate-to-high redshift quasars ( $z \approx 1$ – $5$ ; Page et al. 2001; Vignali et al. 2001; Isaak et al. 2002). The average redshift and submm flux density of the Page et al. (2001) quasars ( $z = 2.1 \pm 0.4$  and  $f_{850\mu\text{m}} = 7.5 \pm 1.6$  mJy) are consistent with those of our SMGs; however, the median X-ray flux of the SMGs is  $\approx 30$  times fainter. The submm properties of quasars are proving to be important from the point of view of the processes of star formation at high redshift and providing clues to the relationship between the formation of SMGs, quasars, and massive galaxies (e.g., Stevens et al. 2003, 2004; Page et al. 2004). However, the X-ray properties of spectroscopically identified SMGs can only be investigated with ultra-deep X-ray observations.

#### 3.2. X-ray Source Classification

Due to the exceptional sensitivity of the 2 Ms CDF-N observations it is possible to detect X-ray emission from star forma-



tion out to high redshift. For example, the soft-band flux limit at the aim point corresponds to  $L_{1.5-6 \text{ keV}} > 8 \times 10^{41} \text{ erg s}^{-1}$  for a galaxy at  $z = 2$ . This luminosity is comparable to those for the most X-ray luminous starburst galaxies in the local Universe (e.g., NGC 3256; Moran et al. 1999; Lira et al. 2002), sources that are bolometrically less energetic than SMGs by  $\approx 1$  order of magnitude. Therefore, the detection of X-ray emission from an SMG does not *a priori* indicate the presence of AGN activity. In order to classify the SMGs in our sample we have used a two-tiered classification procedure. This classification procedure is conservative and may not identify all of the SMGs that host AGN activity. However, we can be confident that any AGN classifications are secure.

The first method of source classification is based on the effective X-ray spectral slope; see Figure 2a. Star-forming galaxies and unobscured AGNs generally have comparatively steep X-ray spectral slopes (i.e.,  $\Gamma \approx 2$ ; e.g., Kim, Fabiano, & Trinchieri 1992a,b; Nandra & Pounds 1994; Ptak et al. 1999; George et al. 2000; Colbert et al. 2004).<sup>5</sup> Obscured AGNs are usually distinguishable from unobscured AGNs and star-forming galaxies by the presence of a flat X-ray spectral slope ( $\Gamma < 1$ ) due to the energy-dependent photo-electric absorption of the X-ray emission (e.g., Maiolino et al. 1998; Risaliti, Maiolino, & Salvati 1999). However, since SMGs are potentially massive galaxies undergoing intense star formation, they could have a large population of high-mass X-ray binaries (HMXBs), which may have comparatively flat X-ray spectral slopes (e.g., neutron star HMXBs can have  $\Gamma \approx 0.5-1.0$ ; Colbert et al. 2004). Eleven of the 17 X-ray detected SMGs have  $\Gamma < 0.5$ , unambiguously indicating the presence of a heavily obscured AGN.

The second method of source classification focuses on the expected X-ray emission from star formation; see Figure 2b. Many studies have shown that the radio luminosity can be used to predict the X-ray luminosity in star-forming galaxies (e.g., Shapley, Fabbiano, & Eskridge 2001; Bauer et al. 2002; Ranalli et al. 2003; Grimm, Gilfanov, & Sunyaev 2003; Gilfanov, Grimm, & Sunyaev 2004; Persic et al. 2004). The main assumption in these predictions is that the radio emission is dominated by star formation; however, the presence of an AGN component to the radio emission will only lead to an overprediction of the contribution from star formation at X-ray energies. The normalisation and slope of these X-ray–radio relationships differ depending upon the relative contributions from low-mass and high-mass X-ray binaries (LMXBs; HMXBs; Gilfanov et al. 2004; Persic et al. 2004; see Figure 2b). Since the properties of SMGs indicate that they are undergoing intense star-formation activity, we only need to consider the contribution from HMXBs (see §4.2). The predicted X-ray emission from star formation in SMGs is large (up to  $L_X \approx 10^{42}-10^{43} \text{ erg s}^{-1}$ ). Even so, all of the sources classified as AGNs show an X-ray excess due to AGN activity; these X-ray excesses will be even greater once the X-ray luminosities are corrected for the effect of absorption. With this second method a further four sources show a clear X-ray excess over that predicted from star formation, indicating that their X-ray emission is dominated by AGN activity. Four of the 10 AGN-classified SMGs with  $> 100$  counts also show some evidence for X-ray variability (M. Paolillo, pri-

<sup>5</sup> Detailed X-ray studies of local star-forming galaxies have shown that they have more complex X-ray spectra than simple power-law emission (e.g., power-law emission and a very soft  $\approx 0.7 \text{ keV}$  thermal component; Ptak et al. 1999); however, at the probable redshifts of our sources the very soft thermal component will be redshifted out of the *Chandra* energy band.

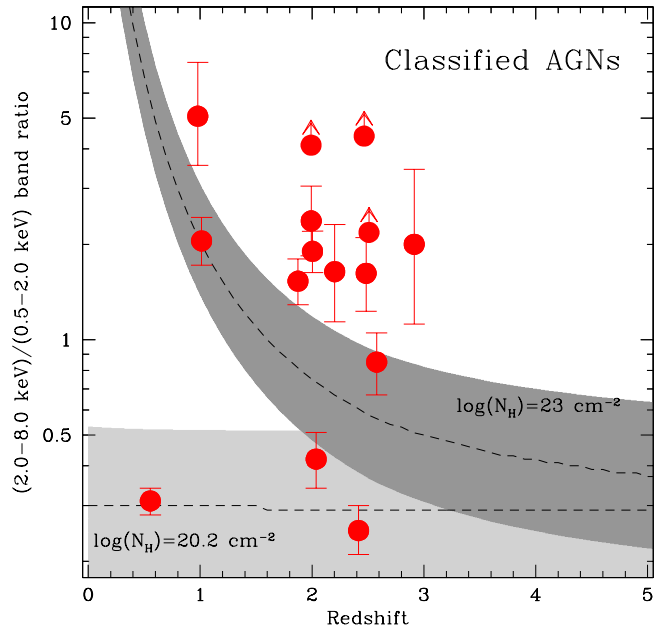


FIG. 3.— X-ray band ratio versus spectroscopic redshift for the X-ray classified AGNs. The light and dark shaded regions show the range of expected band ratios for an unabsorbed and absorbed AGN, respectively. These regions were calculated assuming a  $\Gamma = 1.8 \pm 0.5$  power law with differing amounts of absorption (as shown); these simple AGN models have been calculated using PIMMS Version 3.2d. The error bars correspond to the uncertainties in the band ratio. This simple figure has limited diagnostic utility; however, it suggests that almost all of the AGNs are obscured.

vate communication; see Table 1), a further signature of AGN activity; these constraints are consistent with those found for similarly bright AGNs in the *Chandra* Deep Field-South (Paolillo et al. 2004). None of the sources that have X-ray emission consistent with star formation show evidence for X-ray variability, although the photon statistics are poor.

Overall, the X-ray emission from 15 ( $75^{+25}_{-19}\%$ ) of the 20 SMGs in the sample is AGN dominated. The other five SMGs are the faintest X-ray sources in the sample, and three sources are undetected in the X-ray band (see §2.2). The X-ray emission from these five sources is likely to be dominated by star-formation activity (see §4.2 for further constraints); however, heavily obscured or X-ray weak AGNs cannot be ruled out (e.g., compare with the similar  $z = 2.285$  galaxy FSC 10214+4724; Alexander et al. 2005b). We caution the reader that, due to our sample selection and completeness, these results do not directly indicate a  $\approx 75\%$  AGN fraction in the bright SMG population (the AGN fraction is probably  $> 38^{+12}_{-10}\%$ ; Alexander et al. 2005a, consistent with earlier estimates from the X-ray data; e.g., Alexander et al. 2003b; Borys et al. 2004; Wang, Cowie, & Barger 2004).

### 3.3. X-ray Spectral Analyses

The flat X-ray spectral slopes for the majority of the AGN-classified SMGs indicates the presence of absorption. Basic X-ray absorption constraints can be set using the X-ray band ratio (defined as the ratio of the hard-band to soft-band count rate); see Figure 3. This approach has limited diagnostic utility because AGNs often have more complex spectra than that of power-law emission with differing amounts of absorption. However, it suggests that the majority of the sources are heav-

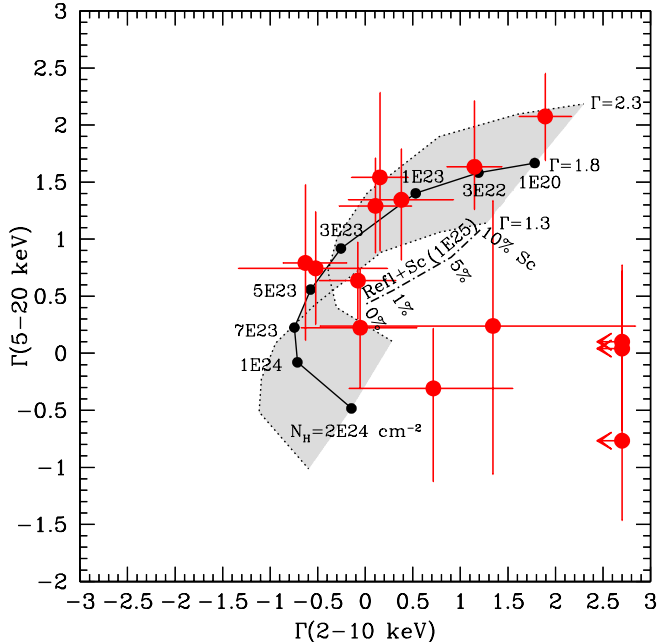


FIG. 4.— Rest-frame 5–20 keV spectral slope versus rest-frame 2–10 keV spectral slope showing the X-ray properties of individual SMGs. The shaded region indicates where typical AGNs with  $\Gamma = 1.8 \pm 0.5$  and  $N_{\text{H}} = 10^{20} - 2 \times 10^{24} \text{ cm}^{-2}$  are expected to lie (individual values of  $N_{\text{H}}$  and  $\Gamma$  are indicated); see §2.3. The dot-dashed line shows where completely Compton-thick AGNs (i.e.,  $N_{\text{H}} \approx 10^{25} \text{ cm}^{-2}$ ; a pure reflection spectrum with ionised gas scattering) with different amounts of scattering (as indicated) are expected to lie; the assumed X-ray spectral slope is  $\Gamma = 1.8$ . This figure shows that the AGN-classified SMGs are well represented by the model, implying that the variations in their X-ray spectral properties are due to absorption.

ily obscured (i.e.,  $N_{\text{H}} \gtrsim 10^{23} \text{ cm}^{-2}$ ). The intrinsic luminosity of the obscured AGNs could be considerably greater than the observed luminosity if the obscuration is high.

In order to estimate the amount of absorption in each of the AGN-classified SMGs more accurately we have constructed a rest-frame power-law diagnostic diagram; see §2.3 and Figure 4. The tracks on this diagram show the approximate regions where typical AGNs are likely to lie; since we investigate rest-frame energies up to 20 keV, CX-OHDFN J123636.7+621156 with a redshift of only  $z = 0.555$  cannot be included in these analyses. The AGN-classified SMGs are clearly well represented by this diagram and, on the basis of our model tracks, 12 ( $\approx 80\%$ ) are heavily obscured ( $N_{\text{H}} \gtrsim 10^{23} \text{ cm}^{-2}$ ). Under the assumption that the different X-ray spectral properties of the SMGs are due to absorption, the lower energy X-ray emission should be more strongly attenuated than the higher energy X-ray emission. This is demonstrated in Figure 5 where the implied attenuations from the luminosity ratios in the 2–10 and 5–20 keV bands are in agreement with those expected from the rest-frame 5–20 keV spectral slopes and the results from Figure 4.

The constraints on the absorption properties of individual sources are comparatively poor. To provide tighter overall constraints we performed joint spectral fitting of all of the sources in the three different obscuration classes indicated in Figure 5 ( $N_{\text{H}} < 10^{23} \text{ cm}^{-2}$ ,  $N_{\text{H}} = 1 - 5 \times 10^{23} \text{ cm}^{-2}$ , and  $N_{\text{H}} > 5 \times 10^{23} \text{ cm}^{-2}$ ). We jointly fitted the rest-frame 2–10 keV and 5–20 keV spectral slopes of the sources, leaving the power-law normalisations as a free parameter for each

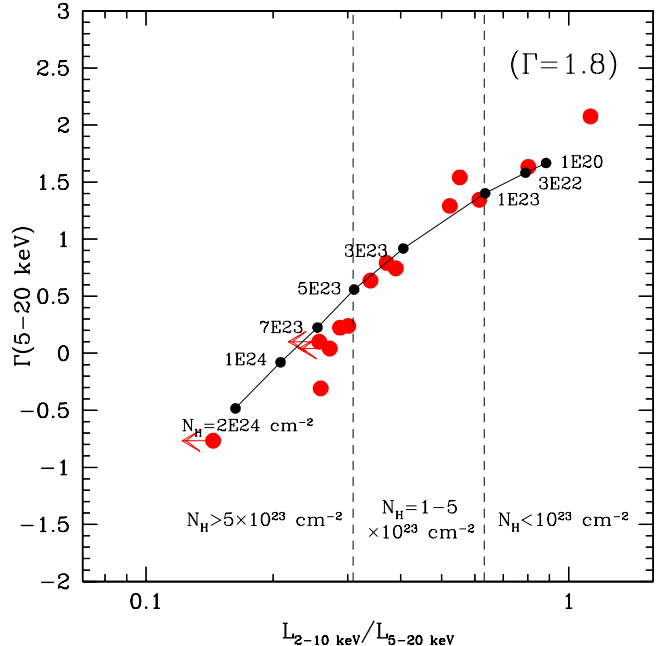


FIG. 5.— Rest-frame 5–20 keV spectral slope versus rest-frame X-ray luminosity ratio ( $L_{2-10\text{keV}}/L_{5-20\text{keV}}$ ). The solid line indicates the track for our adopted AGN model with  $\Gamma = 1.8$  (individual values of  $N_{\text{H}}$  are indicated). The dashed lines indicate the divisions of the three obscuration classes used in the subsequent analyses ( $N_{\text{H}} < 10^{23} \text{ cm}^{-2}$ ,  $N_{\text{H}} = 1 - 5 \times 10^{23} \text{ cm}^{-2}$ , and  $N_{\text{H}} > 5 \times 10^{23} \text{ cm}^{-2}$ ). The implied absorbing column densities of the AGNs in the SMGs are in good agreement with Figure 4.

source. The results of this joint spectral fitting are shown in Figure 6. The average absorbing column densities for the sources in each obscuration class are in excellent agreement with those implied from the individual X-ray spectral analyses. Furthermore, the average intrinsic X-ray spectral slopes estimated from the model tracks ( $\Gamma \approx 1.8$ ) are in good agreement with those found for typical AGNs in the local Universe (e.g., Nandra & Pounds 1994; George et al. 2000).

### 3.4. Rest-frame 2–20 keV spectra

The previous analyses have provided the broad-band X-ray spectral properties of the AGN-classified SMGs but have not been sensitive to discrete emission features (e.g., Fe K $\alpha$  emission). Unambiguous Fe K $\alpha$  emission has not been identified in any of the individual X-ray spectra and, due to poor photon statistics, it is difficult to constrain the X-ray continuum either side of the emission line, which significantly affects the accuracy of Fe K $\alpha$  constraints. It is not possible to improve greatly the Fe K $\alpha$  constraints via joint spectral fitting since the critical parameters are the emission-line and X-ray continuum normalisations, which vary from source to source. However, we can improve the overall signal-to-noise ratio of the spectra by stacking the data for the sources in each obscuration class and searching for the direct signature of Fe K $\alpha$  emission in these composite X-ray spectra.

When combining different X-ray spectra it is important to take into account the effective area and effective exposure of each source. We used XSPEC to output the unbinned X-ray spectrum of each source, folded by its effective area and effective exposure. We then redshift corrected each X-ray spectrum to create a rest-frame spectrum for each source. These

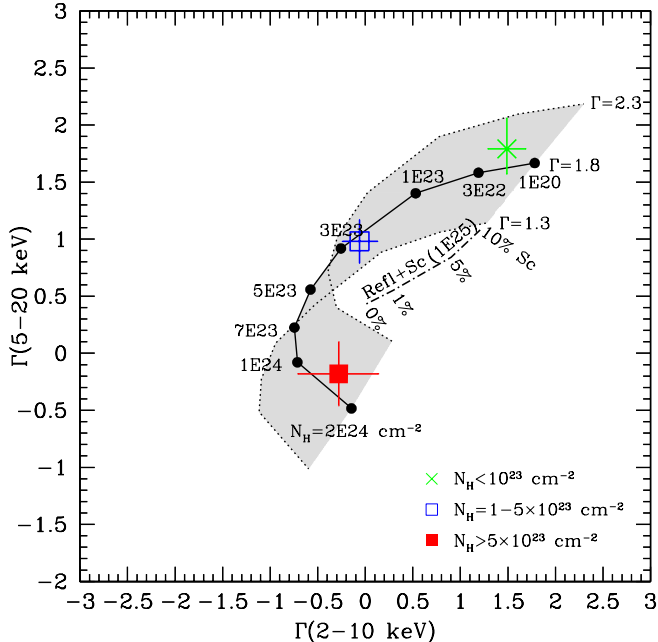


FIG. 6.— Rest-frame 5–20 keV spectral slope versus rest-frame 2–10 keV spectral slope, showing the results of the joint X-ray spectral fitting of the sources in the three obscuration classes from Figure 5. The model tracks are the same as those shown in Figure 4. The average properties of the sources in the three obscuration classes validate the X-ray spectral analyses for individual sources.

rest-frame spectra were combined and then binned to increase the signal-to-noise ratio. Since the spectral response of *Chandra* ACIS-I varies with energy, in principal it is necessary to take into account the spectral response for each source when their spectra are redshifted. However, in the case of our sources the limiting factor is photon statistics rather than spectral resolution (e.g., see §3.3 of Alexander et al. 2003b).

Composite rest-frame 2–20 keV spectra for the three different obscuration classes are shown in Figure 7. The signal-to-noise ratio of these X-ray spectra is significantly higher than the individual X-ray spectra and discrete features and the accurate shape of the X-ray continua can be seen. The obscured AGNs ( $N_{\text{H}} > 10^{23} \text{ cm}^{-2}$ ) show a clear deficit of emission at  $\lesssim 5 \text{ keV}$  due to absorption. As expected, there is a good correspondence between the amount of absorption and obscuration class. We plotted the model spectra determined from the joint X-ray spectral fitting (see Figure 6 and §3.3) and normalised them to the composite X-ray spectra by eye; see Figure 7. Reassuringly, the model tracks provide a good description of the composite X-ray spectra, validating the results from the X-ray spectral analyses (Figures 3–6) and showing that the variations in the properties of the individual X-ray spectra are due to absorption.

An emission feature at the rest-frame energy of Fe  $K\alpha$  is seen in the composite spectrum of the most heavily obscured AGNs ( $N_{\text{H}} > 5 \times 10^{23} \text{ cm}^{-2}$ ); see Figure 7. The rest-frame equivalent width of this feature ( $\approx 1 \text{ keV}$ ) is consistent with that expected for Compton-thick or near Compton-thick AGNs (e.g., Bassani et al. 1999) and suggests that some of the X-ray emission is reflected and/or scattered (e.g., Matt, Brandt, & Fabian 1996). The rest-frame energy of this feature is closer to 6.7 keV than 6.4 keV, possibly indicating that it is produced in a warm scattering medium rather than from cold reflection, or that contributions from both are present.

However, given the poor signal-to-noise ratio and effective spectral resolution of the data, we cannot distinguish between these possibilities (e.g., compare the different signal-to-noise ratio spectra of NGC 1068 and NGC 2992 in Figure 4 of Turner et al. 1997a). If all of the X-ray emission was reflected/scattered then we would not be able to get an accurate estimate of the intrinsic X-ray luminosity of the AGNs in this obscuration class. However, at least for the properties of our model, a significant fraction of the direct X-ray emission is seen at  $\gtrsim 10 \text{ keV}$ , providing a reasonable constraint on the underlying AGN luminosity. There is ambiguous evidence for Fe  $K\alpha$  in the composite spectra of the  $N_{\text{H}} < 5 \times 10^{23} \text{ cm}^{-2}$  sources, potentially indicating the presence of Compton-thick or near Compton-thick AGN emission that is additionally obscured by starburst regions (e.g., Fabian et al. 1998). Improved photon statistics are required to test this scenario; see §4.4.

In Figure 7 there appears to be an excess of  $< 4 \text{ keV}$  emission with respect to the model in the composite spectrum of the most heavily obscured sources ( $N_{\text{H}} > 5 \times 10^{23} \text{ cm}^{-2}$ ), which may be due to star formation. The extrapolated  $\approx 0.5$ – $8.0 \text{ keV}$  luminosity ( $\approx 10^{42} \text{ erg s}^{-1}$ ) is consistent with the X-ray properties of the SMGs individually classified as starburst galaxies; see Table 1 and §3.2. We further investigate the X-ray emission from star formation in §4.2.

### 3.5. Absorption Correction

Since accurate absorption corrections are challenging to determine even for well-studied obscured AGNs in the local Universe (e.g., Turner et al. 1997b; Bassani et al. 1999; Matt et al. 2000), the absorption corrections for our X-ray faint SMGs will be somewhat uncertain. Thankfully, the composite X-ray spectra have shown that our AGN model gives a good characterisation of the X-ray properties of the AGN-classified SMGs and therefore provides a good base for determining plausible absorption corrections. In Table 2 we show our estimated unabsorbed X-ray luminosities for each of the AGN-classified SMGs using our AGN model and the column-density constraints from Figures 4–5. Although the absorption corrections for the most heavily obscured objects ( $N_{\text{H}} > 5 \times 10^{23} \text{ cm}^{-2}$ ) are the most uncertain, they are consistent with those previously estimated for similar sources with comparable column densities and reflection/scattering components (e.g., Iwasawa et al. 2001, 2005b; Fabian et al. 2003; Wilman et al. 2003). Perhaps reassuringly, the mean unabsorbed luminosities of the  $N_{\text{H}} > 5 \times 10^{23} \text{ cm}^{-2}$  sources are consistent with those found for the  $N_{\text{H}} = 1$ – $5 \times 10^{23} \text{ cm}^{-2}$  sources ( $L_{\text{X}} \approx 6 \times 10^{43} \text{ erg s}^{-1}$  versus  $L_{\text{X}} \approx 5 \times 10^{43} \text{ erg s}^{-1}$ ), as expected if the differing amounts of absorption are primarily due to the orientation of the obscuration with respect to the central source (i.e., the unified AGN model; Antonucci 1993). To provide a comparison to further studies in the literature (e.g., Bautz et al. 2000; Mainieri et al. 2002; Szokoly et al. 2004; Severgnini et al. 2005), we also calculated unabsorbed X-ray luminosities under the assumption of a simple absorbed power-law model (i.e., without the reflection and scattering components); see Table 2. However, we note that this model is unable to explain the presence of Fe  $K\alpha$  emission in the most heavily obscured AGNs.

Although our X-ray observations probe rest-frame energies  $\gtrsim 20 \text{ keV}$ , it is possible that a large fraction of the X-ray emission is still hidden (e.g., much of the observed emission could be scattered rather than direct). More sensitive X-ray observations, and observations at  $> 10$ –

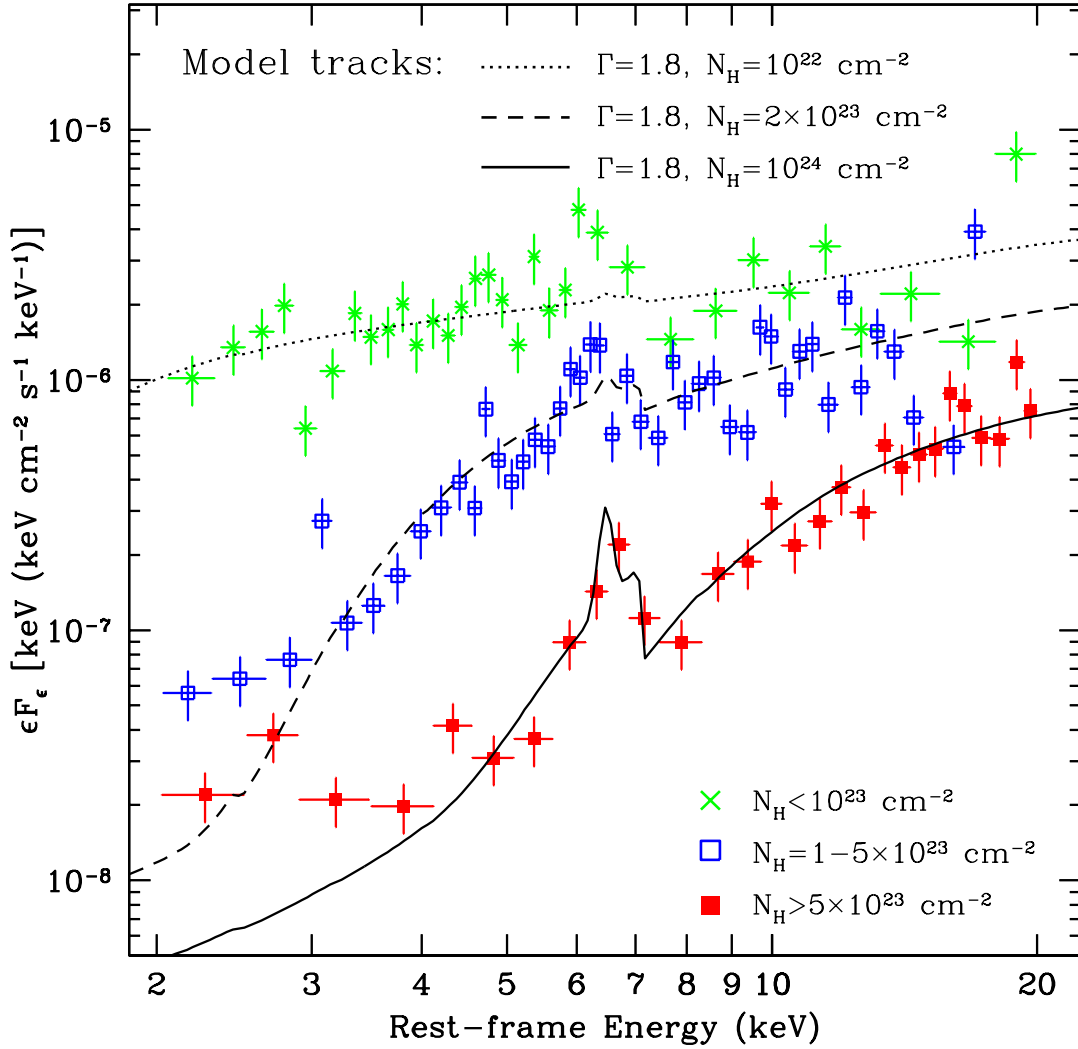


FIG. 7.— Composite rest-frame 2–20 keV spectra for each obscuration class, as indicated; see §3.3. The spectra are normalised to the average flux density of each obscuration class (with the exception of the the  $N_{\text{H}} < 10^{23} \text{ cm}^{-2}$  sources, which have been scaled by a factor of 2 for presentation purposes) and are binned at 20 counts per bin. The total number of counts for each obscuration class are  $\approx 690$  ( $N_{\text{H}} < 10^{23} \text{ cm}^{-2}$ ),  $\approx 990$  ( $N_{\text{H}} = 1-5 \times 10^{23} \text{ cm}^{-2}$ ), and  $\approx 580$  ( $N_{\text{H}} > 5 \times 10^{23} \text{ cm}^{-2}$ ). The different line styles show the X-ray spectra for our adopted model for different amounts of X-ray absorption; the absorbing column density is taken from the joint X-ray spectral fitting for each obscuration class (see Figure 6). The Fe K $\alpha$  line is at 6.4 keV in the model spectra; the apparent emission feature bluewards of the Fe K $\alpha$  line is due to the supposition of the different continuum components and the Fe absorption edge at  $\approx 7.1$  keV. The apparent excess of  $< 4$  keV emission, with respect to the model, in the composite spectrum of the most heavily obscured sources ( $N_{\text{H}} > 5 \times 10^{23} \text{ cm}^{-2}$ ) may be due to star formation (see §3.4).

20 keV (observed-frame energies), would be able to test this scenario (e.g., see Franceschini et al. 2000; Iwasawa et al. 2001 for the brighter but similarly luminous galaxy IRAS 09104+4109). Significant high-energy constraints could become available with NuSTAR as soon as 2009, before further constraints with *Constellation-X* and *XEUS* in  $> 10$  yrs time (see §4.4).<sup>6</sup> An alternative approach is to seek independent estimates of the AGN luminosity at other wavelengths (e.g., via the [OIII] $\lambda 5007$  emission line or any strong near-IR to mid-IR high-excitation lines; Mulchaey

et al. 1994; Bassani et al. 1999; Sturm et al. 2002). Only one of our AGN-classified SMGs has an independent AGN luminosity constraint ([OIII] emission is detected from CXO-HDFN J123549.4+621536; T. Takata, in preparation). The predicted rest-frame 0.5–8.0 keV luminosity of this source ( $L_{\text{X}} \approx 0.1-10 \times 10^{44} \text{ erg s}^{-1}$ , determined using the [OIII]–X-ray relationship given in Bassani et al. 1999) is consistent with our estimate ( $L_{\text{X}} \approx 10^{44} \text{ erg s}^{-1}$ ); however, there are large uncertainties and this estimate is likely to increase when the effect of host-galaxy absorption towards the [OIII] emission-line region is taken into account. Further independent estimates of the AGN luminosity in SMGs would provide tighter constraints on the amount of nuclear absorption; see also §4.3.

<sup>6</sup> On the basis of the expected  $\approx 3 \sigma$  sensitivity limits for an ultra-deep  $\approx 1$  Ms exposure (10–40 keV fluxes of  $\approx 10^{-14} \text{ erg cm}^{-2} \text{ s}^{-1}$ ; D. Stern, private communication), NuSTAR should detect emission down to  $L_{\text{X}} \approx 10^{44}-10^{45} \text{ erg s}^{-1}$  at  $z \approx 1-3$ ; see <http://www.nustar.caltech.edu/> for further details.



## 4. DISCUSSION

The analyses in §3 have provided a comprehensive characterisation of the X-ray properties of radio-selected spectroscopically identified SMGs with  $f_{850\mu\text{m}} \gtrsim 4$  mJy. These properties can be used to explore the role of AGN activity in these galaxies. In §4.1 we further investigate the AGN properties of our SMG sample, in §4.2 we estimate the contribution that AGN activity makes to the bolometric luminosity, in §4.3 we consider the constraints on black-hole growth, and in §4.4 we discuss the prospects for deeper X-ray observations and explore the scientific potential of the next generation of X-ray observatories for the study of SMGs.

## 4.1. AGN Activity in the SCUBA Galaxy Sample

The X-ray properties of the AGN-classified SMGs in our sample are generally consistent with those of nearby luminous AGNs (i.e.,  $\Gamma \approx 1.8 \pm 0.5$ ,  $N_{\text{H}} \approx 10^{20}\text{--}10^{24}$  cm $^{-2}$ , and  $L_{\text{X}} \approx 10^{43}\text{--}10^{44.5}$  erg s $^{-1}$ ; e.g., Smith & Done 1996; Turner et al. 1997b; Maiolino et al. 1998; Risaliti et al. 1999); see §3 and Table 2. The majority ( $\approx 80\%$ ) of the AGNs are heavily obscured ( $N_{\text{H}} \gtrsim 10^{23}$  cm $^{-2}$ ), four of which have  $L_{\text{X}} \gtrsim 10^{44}$  erg s $^{-1}$  and could be considered obscured (Type 2) quasars; see Bautz et al. (2000) and Mainieri et al. (2005a) for other examples of obscured quasars that are bright at submm wavelengths. With the exception of completely Compton-thick AGNs (i.e.,  $N_{\text{H}} \approx 10^{25}$  cm $^{-2}$ ), the overall column density distribution would be roughly similar to that found for nearby AGNs (e.g., Risaliti et al. 1999; Salvati & Maiolino 2000). The lack of obvious X-ray emission from AGN activity in the X-ray classified starbursts could be because the AGNs are of a low luminosity ( $L_{0.5\text{--}8.0\text{ keV}} \lesssim 10^{42}$  erg s $^{-1}$ ) or are completely Compton thick ( $N_{\text{H}} \approx 10^{25}$  cm $^{-2}$ ).<sup>7</sup> Interestingly, if the latter is assumed then the estimated column density distribution would be remarkably similar to that found for nearby AGNs.

The obscured AGN fraction in our sample ( $\approx 80\%$  have  $N_{\text{H}} \gtrsim 10^{23}$  cm $^{-2}$ ) is larger than that found from identification studies of the  $\approx 2\text{--}8$  keV background population (e.g., Ueda et al. 2003 find similar numbers of obscured and unobscured AGNs; see also Barger et al. 2002; Mainieri et al. 2002; Szokoly et al. 2004). Although this may suggest a prevalence for obscured activity in the SMG population, selection effects are also likely to be at least partially responsible. For example, due to the comparatively high redshifts of our sources we probe considerably higher rest-frame energies than those for the bulk of the spectroscopically identified sources in deep X-ray surveys [e.g.,  $\approx 1.5\text{--}24$  keV (at  $z \approx 2$ ) as compared to  $\approx 0.9\text{--}14$  keV (at  $z \approx 0.7$ ) at observed energies of  $0.5\text{--}8.0$  keV], allowing higher column densities to be penetrated. Further  $z > 1$  obscured AGNs are likely to have been detected in X-ray surveys but lack spectroscopic redshifts due to the faintness of their optical counterparts (e.g., Alexander et al. 2001; Barger et al. 2002; Fiore et al. 2003; Treister et al. 2004; Mainieri et al. 2005b). These optically faint X-ray sources are the dominant population of obscured AGNs at  $z > 1$  and may account for as much as  $\approx 50\%$  of the AGNs detected in deep X-ray surveys (Alexander et al. 2002). Complete spectroscopic identification of these sources is required to determine the obscured to unobscured AGN ratio at  $z > 1$

<sup>7</sup> Of course some of the X-ray classified starbursts may not host AGN activity. However, we note that the similar  $z = 2.285$  galaxy FSC 10214+4724 hosts an AGN that is weak at X-ray energies and would have been classified as a starburst galaxy in our study (Alexander et al. 2005b).

and reveal whether our X-ray detected SMGs are preferentially more obscured than the general  $z > 1$  X-ray source population.

## 4.2. What Powers SCUBA Galaxies?

AGN activity clearly plays an important role in the spectroscopically identified SMG population but does it dominate the bolometric output? The answer to this key question can have important implications for the formation and evolution of massive galaxies and the growth of massive black holes (see §1). As found for most dusty luminous galaxies, the luminosity of SMGs is likely to peak at far-IR wavelengths and have components of both AGN and star-formation activity (e.g., Sanders & Mirabel 1996; Genzel & Cesarsky 2000). Many studies have suggested that star formation accounts for a large fraction of the bolometric output of SMGs (e.g., Frayer et al. 1998, 2004; Ivison et al. 2002, 2004; Alexander et al. 2003b; Almaini et al. 2003; Chapman et al. 2004a; Egami et al. 2004; Swinbank et al. 2004) but none has resolved the rest-frame far-IR emission. The most direct study to date is that of Chapman et al. (2004a) who showed that  $\approx 70\%$  of radio-identified SMGs have radio emission extended on  $\approx 10$  kpc scales, implying that the rest-frame far-IR emission is also extended over these scales. However, these results do not rule out the presence of energetically significant AGN components on smaller scales. The important contribution our study can make to this debate is in providing direct estimates of the bolometric contribution from AGN activity.

In Figure 8 we show the rest-frame far-IR luminosity versus unabsorbed  $0.5\text{--}8.0$  keV luminosity for the SMGs and compare them to well-studied starburst galaxies and AGNs drawn from the literature. The shaded region indicates the typical range of luminosity ratios for the well-studied quasars of Elvis et al. (1994) and provides an indication of the location of AGN-dominated sources on this figure. None of the far-IR luminous SMGs ( $L_{\text{FIR}} \gtrsim 10^{12} L_{\odot}$ ) lies within the dark-shaded region, indicating that they are comparatively weak at X-ray energies. The difference between the median X-ray-to-far-IR luminosity ratios of the AGN-classified SMGs ( $\frac{L_{\text{X}}}{L_{\text{FIR}}} \approx 0.004$ )

and the quasars ( $\frac{L_{\text{X}}}{L_{\text{FIR}}} \approx 0.05$ ) suggest that the AGN activity in the SMGs contributes, on average, only  $\approx 8\%$  of the far-IR emission. This comparison indicates that star formation typically dominates the bolometric output of these SMGs. However, if the SMGs have an AGN dust-covering factor  $\approx 12$  times larger than found in the quasars then they could potentially be AGN dominated (i.e., a larger amount of dust could be heated for a given central source luminosity). Although the large fraction of obscured AGNs in our sample suggests that the dust-covering factor is large in these SMGs, the dust-covering factor of quasars is uncertain and may depend on the evolutionary state or nature of individual objects (e.g., Haas et al. 2003; Page et al. 2004).

We can take a different approach and compare our SMGs to the literature galaxies, many of which host an obscured AGN and may be physically similar to the SMGs; see Figure 8. The complication of this comparison is that the relative contribution from AGN and star-formation activity in these galaxies is often poorly constrained. Even so, we can gain some insight into the relative dominance of AGN and star-formation activity by “calibrating” Figure 8 using the *ISO* mid-IR spectral diagnostics of Rigopoulou et al. (1999) and Tran et al. (2001); see also Genzel et al. (1999) and Lutz, Veilleux, & Genzel (1999). On the basis of these studies, we have found that the



AGN and star-formation activity in these SMGs (e.g., Lutz et al. 2005 for the first constraints). However, significantly improved constraints are unlikely to be achieved before the advent of the Atacama Large Millimeter Array (ALMA), which will offer spatial resolution constraints at submm wavelengths on  $\approx 100$  pc scales for galaxies at  $z \approx 2$ .<sup>8</sup>

In Figure 8 we also show the X-ray and far-IR luminosities of the starburst-classified SMGs. The mean X-ray-to-far-IR luminosity ratio of these sources ( $\frac{L_X}{L_{\text{FIR}}} \approx 10^{-4}$ , when the X-ray stacking result of the three X-ray undetected SMGs is included; see §2.2) is consistent with that expected from star formation if the X-ray emission is dominated by HMXBs (Persic et al. 2004; see also Figure 2b and §3.2). Under this assumption the X-ray derived star-formation rates ( $\approx 1300$ – $2700 M_{\odot}\text{yr}^{-1}$ ) are in good agreement with those determined using other techniques (e.g., Swinbank et al. 2004; Chapman et al. 2005). The mean X-ray-to-far-IR luminosity ratio is  $\approx 4$  times lower than that found for typical starburst galaxies in the local Universe. However, as argued in Persic et al. (2004; see also Franceschini et al. 2003), the X-ray emission from typical starburst galaxies will be dominated by long-lived LMXBs, which will be comparatively weak in intense star-forming galaxies. Of course, the weak X-ray emission from these sources could also imply that luminous completely Compton-thick AGNs are present (e.g., Iwasawa et al. 2005a).

#### 4.3. Growth of Black Holes in Massive Star-Forming Galaxies

In Alexander et al. (2005a) we used the results presented here to constrain the growth of black holes in massive star-forming galaxies. We showed that the AGN fraction in the bright SMG population is  $> 38^{+12}_{-10}\%$ , when corrected for bright SMGs without spectroscopic redshifts, and argued that this indicates that their black holes are almost continuously growing throughout vigorous star-formation episodes. The most likely catalyst for this activity appeared to be galaxy major mergers (e.g., Chapman et al. 2003c; Conselice et al. 2003). Shortly after the completion of our study sophisticated hydrodynamical simulations of galaxy major mergers, taking into account the growth of both the black hole and stellar components, were published (e.g., Di Matteo et al. 2005; Springel et al. 2005). The simulation results are in good agreement with the conclusions of Alexander et al. (2005a), with the peak epoch of star formation corresponding to a heavily obscured rapid black-hole growth phase, which is ultimately preceded by an unobscured quasar phase (Hopkins et al. 2005). However, the black holes of the most massive galaxies in these simulations (which are probably most similar to the SMGs) are up-to an order of magnitude more massive than those estimated from our X-ray luminosities under the assumption of Eddington-limited accretion ( $M_{\text{BH(Edd)}} \lesssim 10^8 M_{\odot}$ ). Our results can be better reconciled with the simulations if either the black holes in the AGN-classified SMGs are accreting at sub-Eddington rates, a large fraction of the AGN activity is hidden at rest-frame energies of  $\approx 20$  keV (see §3.5), or the X-ray-to-bolometric luminosity ratio is significantly lower than that typically assumed for AGNs (i.e., Elvis et al. 1994; see Table 1 of Alexander et al. 2005a for further details). However, there is further observational evidence that the masses of the black holes in SMGs may be comparatively modest and in good agreement

with our estimate. Rest-frame optical spectra of SMGs show that when broad emission lines are detected they are often comparatively narrow (typical full width at half-maximum velocities of  $\approx 1000$ – $3000 \text{ km}^{-1}$ ; Vernet & Cimatti 2001; Smail et al. 2003; Swinbank et al. 2004, 2005; T. Takata et al., in preparation). Under the assumption that the dynamics of the broad-line regions in these sources are dominated by the gravity of the central black hole, these comparatively narrow emission line widths suggest typical black-hole masses of  $\lesssim 10^8 M_{\odot}$  for mass accretion rates of  $\lesssim 1 M_{\odot} \text{ yr}^{-1}$  (Alexander et al. 2005a; e.g., McLure & Dunlop 2004). Although it is premature to draw conclusions before more accurate black-hole mass constraints are secured, we note that other models have suggested that the masses of the black holes in SMGs are comparatively modest (e.g., Archibald et al. 2002; Kawakatu et al. 2003; Granato et al. 2004a,b). In particular, the physically motivated models of Granato et al. bear a striking similarity to our results (see Figures 2 & 3 in Granato et al. 2004b for the  $M_{\text{vir}} = 10^{12.4} M_{\odot}$  model).

#### 4.4. Prospects for Deeper X-ray Observations

The quality of the individual X-ray spectra are restricted by poor photon statistics. However, the composite X-ray spectra in §3.4 demonstrate what could be achieved for individual sources with extremely long *Chandra* exposures (up to  $\approx 12$  Ms). With individual X-ray spectra of this quality we would be able to significantly improve the constraints for individual sources (e.g.,  $\Gamma$ ,  $N_{\text{H}}$ , the strength of Fe K $\alpha$  emission, intrinsic X-ray luminosity, measure soft X-ray excesses due to star-formation activity). The increased photon statistics would also allow for basic X-ray spectral analyses (up to  $\approx 200$  counts) of the starburst-classified SMGs.

The major scientific thrust of the next generation of X-ray observatories (*Constellation-X* and *XEUS*) is high-resolution spectroscopy of faint X-ray sources.<sup>9</sup> In order to investigate the scientific potential of these observatories for the study of SMGs, we have simulated a 300 ks *XEUS* exposure of one of the most heavily obscured sources (SMMJ 123622.6+621629 at  $z = 2.466$ ) using XSPEC; see Figure 9. An Fe K $\alpha$  emission line is easily identifiable at rest-frame 6.4 keV, indicating that this is a Compton-thick or near Compton-thick AGN; similar results can be obtained with *Constellation-X* for sources  $\approx 10$  times brighter. The quality (signal-to-noise ratio and spectral resolution) of the simulated X-ray spectrum exceeds that of our composite X-ray spectra (compare with Figure 7). Both *Constellation-X* and *XEUS* will also have the capability to detect sources at  $> 10$ – $20$  keV (observed-frame energies) and place crucial AGN luminosity constraints at very high X-ray energies (see Footnote 6 for NuSTAR constraints); see §3.5.

The increased photon statistics and spectral resolution of the next-generation X-ray observatories should allow for the detection of weaker AGN features. For example, some local AGNs and powerful quasars have shown evidence for large-scale outflowing material, probably due to accretion-disk winds (e.g., Chartas et al. 2002; Kaspi et al. 2002; Ogle et al. 2003). These outflows provide an efficient method for distributing high-metallicity gas into the intergalactic medium and may be responsible for producing the  $M$ – $\sigma$  relationship seen in local galaxies (e.g., Silk & Rees 1998; Fabian 1999; King 2003; Di Matteo et al. 2005). If SMGs are the precursors to luminous quasar activity, and the ancestors of nearby

<sup>8</sup> See <http://www.alma.nrao.edu/> for more details on ALMA.

<sup>9</sup> See <http://constellation.gsfc.nasa.gov/science/index.html> and <http://www.rssd.esa.int/XEUS/> for more details.

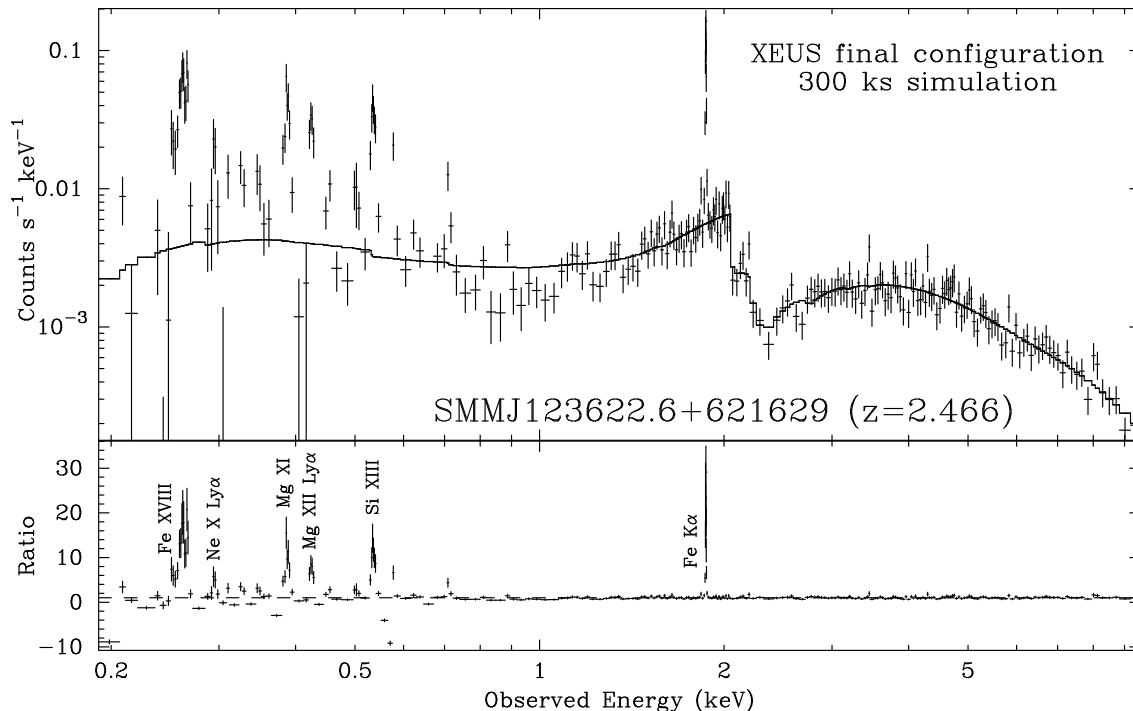


FIG. 9.— Simulated 300 ks final-configuration *XEUS* spectrum of the heavily obscured source SMMJ 123622.6+621629 (top panel). The spectrum was simulated using our adopted AGN model (see §2.3) with  $\Gamma = 1.8$  and  $N_{\text{H}} = 1.5 \times 10^{24} \text{ cm}^{-2}$ , and additionally includes an accretion-disk wind outflow [taken from NGC 1068 (Ogle et al. 2003) and scaled to the Fe  $K\alpha$  flux of our source]; see §4.4. The solid line indicates the input model with the emission-line components removed to highlight the emission-line features. The bottom panel shows the ratio of the simulated data to the model. Rest-frame 6.4 keV Fe  $K\alpha$  is easily identified (at  $\approx 1.8$  keV) and indicates that this source is a Compton-thick or near Compton-thick AGN. The  $< 1$  keV emission features are due to the outflowing accretion-disk wind. Six of the strongest emission lines are labelled in the bottom panel (see Ogle et al. 2003 for further information and line identifications).

massive galaxies, then they are likely to produce significant emission-line outflows (see Smail et al. 2003; Chapman et al. 2004b; Swinbank et al. 2005 for evidence at optical/near-IR wavelengths). We included the emission-line outflow parameters found for NGC 1068 (Ogle et al. 2003) to our simulated 300 ks *XEUS* spectrum, scaled to the Fe  $K\alpha$  flux of our source; see Figure 9. The emission-line signatures of the outflow are identifiable in the simulated spectrum at  $\lesssim 1$  keV, allowing basic constraints to be placed on the properties of the outflowing material (e.g., the mass outflow rate). These constraints could prove to be crucial in our understanding of the connection between AGN and star-formation activity at high redshift, and help to explain the properties of nearby massive galaxies.

## 5. CONCLUSIONS

Using the powerful combination of ultra-deep X-ray observations and deep optical spectroscopic data we have placed constraints on the X-ray properties of 20 radio-selected spectroscopically identified SMGs with  $f_{850\mu\text{m}} \gtrsim 4$  mJy. Our key results are the following:

1. Seventeen of the 20 SMGs in our sample are detected at X-ray energies. From a classification of their X-ray properties, we found the X-ray emission to be dominated by AGN activity in 15 sources ( $\approx 75\%$ ); the X-ray emission from the other 5 sources is likely to be dominated by star-formation activity. See §3.2.
2. Using a variety of X-ray spectral analyses we found that the properties of the AGNs are generally consistent with those of nearby luminous AGNs

(i.e.,  $\Gamma \approx 1.8 \pm 0.5$ ,  $N_{\text{H}} \approx 10^{20}\text{--}10^{24} \text{ cm}^{-2}$ , and  $L_{\text{X}} \approx 10^{43}\text{--}10^{44.5} \text{ erg s}^{-1}$ ); see §3 and Table 2. The majority ( $\approx 80\%$ ) of the AGNs are heavily obscured ( $N_{\text{H}} \gtrsim 10^{23} \text{ cm}^{-2}$ ), four of which have  $L_{\text{X}} \gtrsim 10^{44} \text{ erg s}^{-1}$  and could be considered obscured quasars. The estimated column-density distribution is roughly similar to that found for nearby AGNs. See §3.3 and §4.1.

3. We constructed rest-frame 2–20 keV composite spectra for three different obscuration classes ( $N_{\text{H}} < 10^{23} \text{ cm}^{-2}$ ,  $N_{\text{H}} = 1\text{--}5 \times 10^{23} \text{ cm}^{-2}$ , and  $N_{\text{H}} > 5 \times 10^{23} \text{ cm}^{-2}$ ). These composite spectra revealed features not observed in the individual X-ray spectra and an  $\approx 1$  keV equivalent width Fe  $K\alpha$  emission line is seen in the composite X-ray spectrum of the most heavily obscured AGNs, suggesting Compton-thick or near Compton-thick absorption. The good agreement between our model tracks and the composite X-ray spectra validate the X-ray spectral analyses of individual sources. See §3.4.
4. Taking into account the effects of absorption, we found that the average X-ray to far-IR luminosity ratio of the AGN-classified sources ( $\frac{L_{\text{X}}}{L_{\text{FIR}}} = 0.004$ ) is approximately one order of magnitude below that found for typical quasars. This result suggests that intense star-formation activity (of order  $\approx 1000 M_{\odot} \text{ yr}^{-1}$ ) dominates the bolometric output of spectroscopically identified SMGs. Possible biases in the selection of this sample (see §2.1) would suggest that, if anything, they

should have a higher AGN contribution than spectroscopically unidentified SMGs. We also investigated the possibility that the X-ray to far-IR luminosity ratio for the AGNs in SMGs is intrinsically less than that found for typical quasars and postulated that some SMGs may be AGN dominated. See §4.2.

5. We found that the X-ray emission from the starburst-classified SMGs is consistent with that expected from HMXBs. The X-ray derived star-formation rates ( $\approx 1300\text{--}2700 M_{\odot}\text{yr}^{-1}$ ) are in good agreement with those determined using other techniques. See §4.2.
6. We find good agreement between our overall picture for the growth of black holes in massive galaxies and the results from recent hydrodynamic simulations. We provide support that the black holes in our AGN-classified SMGs are  $\lesssim 10^8 M_{\odot}$ . See §4.3.
7. We demonstrated that the next generation of X-ray observatories (*Constellation-X* and *XEUS*) will place significantly improved X-ray spectral constraints on individual sources. In addition to constraining the absorption properties of the AGN components we found that these X-ray observatories have the potential to de-

tect the presence and properties of outflowing material. These observations could prove to be crucial in our understanding of the evolution of massive galaxies. See §4.4.

## ACKNOWLEDGMENTS

We acknowledge support provided by the Royal Society (DMA, IS), PPARC (FEB), NASA #9174 (SSC), NSF award AST-0205937, the Research Corporation, and the Alfred P. Sloan Foundation (AWB), NSF CAREER award AST-99833783, and CXC grant G02-3187A (WNB). We are grateful to Stefan Immler for performing the X-ray stacking analyses on the X-ray undetected SCUBA galaxies. We thank Omar Almaini, Tiziana Di Matteo, Andy Fabian, Reinhard Genzel, John Grimes, Gunther Hasinger, Kazushi Iwasawa, Pat Ogle, Maurizio Paolillo, Andy Ptak, Nick Scoville, Dan Stern, Tadafumi Takata, and Cristian Vignali for useful comments and suggestions. We thank the referee for presentation suggestions. This research has made use of the NASA/IPAC Extragalactic Database (NED) which is operated by the Jet Propulsion Laboratory, California Institute of Technology, under contract with the National Aeronautics and Space Administration.

## REFERENCES

- Alexander, D. M., Brandt, W. N., Hornschemeier, A. E., Garmire, G. P., Schneider, D. P., Bauer, F. E., & Griffiths, R. E. 2001, *AJ*, 122, 2156
- Alexander, D. M., Bauer, F. E., Brandt, W. N., Hornschemeier, A. E., Vignali, C., Garmire, G. P., & Schneider, D. P. 2002, *New Visions of the X-ray Universe in the XMM-Newton and Chandra Era*, ESTEC, The Netherlands, submitted (astro-ph/0202044)
- Alexander, D. M., et al. 2003a, *AJ*, 126, 539
- Alexander, D. M., et al. 2003b, *AJ*, 125, 383
- Alexander, D. M., et al. 2005a, *Nature*, 434, 738
- Alexander, D. M., Chartas, G., Bauer, F. E., Brandt, W. N., Simpson, C., & Vignali, C. 2005b, *MNRAS*, 357, L16
- Almaini, O. 2003, *Astronomische Nachrichten*, 324, 109
- Almaini, O., et al. 2003, *MNRAS*, 338, 303
- Antonucci, R. 1993, *ARA&A*, 31, 473
- Archibald, E. N., Dunlop, J. S., Jimenez, R., Friaça, A. C. S., McLure, R. J., & Hughes, D. H. 2002, *MNRAS*, 336, 353
- Arnaud, K. A. 1996, in *ASP Conf. Ser. 101, Astronomical Data Analysis Software and Systems V*, eds. Jacoby G. & Barnes J. (San Francisco: ASP), 17
- Arnaud, K. A. 2002, *ApJ*, submitted
- Avni, Y. 1976, *ApJ*, 210, 642
- Barger, A. J., Cowie, L. L., Brandt, W. N., Capak, P., Garmire, G. P., Hornschemeier, A. E., Steffan, A. T., & Wehner, E. H. 2002, *AJ*, 124, 1839
- Barger, A. J., Cowie, L. L., & Sanders, D. B. 1999, *ApJ*, 518, L5
- Barger, A. J., Cowie, L. L., Smail, I., Ivison, R. J., Blain, A. W., & Kneib, J.-P. 1999, *AJ*, 117, 2656
- Barger, A. J., Cowie, L. L., Mushotzky, R. F., & Richards, E. A. 2001a, *AJ*, 121, 662
- Barger, A. J., Cowie, L. L., Steffan, A. T., Hornschemeier, A. E., Brandt, W. N., & Garmire, G. P. 2001b, *ApJ*, 560, L23
- Bassani, L., Dadina, M., Maiolino, R., Salvati, M., Risaliti, G., della Ceca, R., Matt, G., & Zamorani, G. 1999, *ApJS*, 121, 473
- Bauer, F. E., Alexander, D. M., Brandt, W. N., Hornschemeier, A. E., Vignali, C., Garmire, G. P., & Schneider, D. P. 2002, *AJ*, 124, 2351
- Bautz, M. W., Malm, M. R., Baganoff, F. K., Ricker, G. R., Canizares, C. R., Brandt, W. N., Hornschemeier, A. E., & Garmire, G. P. 2000, *ApJ*, 543, L119
- Blackburn, J. K. 1995, *ASP Conf. Ser. 77: Astronomical Data Analysis Software and Systems IV*, 4, 367
- Blain, A. W., Kneib, J.-P., Ivison, R. J., & Smail, I. 1999, *ApJ*, 512, L87
- Blain, A. W., Smail, I., Ivison, R. J., Kneib, J.-P., & Frayer, D. T. 2002, *Physics Reports*, 369, 111
- Blain, A. W., Chapman, S. C., Smail, I., & Ivison, R. 2004a, *ApJ*, 611, 52
- Blain, A. W., Chapman, S. C., Smail, I., & Ivison, R. 2004b, *ApJ*, 611, 725
- Borys, C., et al. 2003, *MNRAS*, 344, 385
- Borys, C., Scott, D., Chapman, S., Halpern, M., Nandra, K., & Pope, A. 2004, *MNRAS*, 355, 485
- Braito, V., et al. 2003, *A&A*, 398, 107
- Braito, V., et al. 2004, *A&A*, 420, 79
- Brandt, W. N., et al. 2001, *AJ*, 122, 2810
- Brandt, W. N., & Hasinger, G. 2005, *ARA&A*, in press (astro-ph/0501058)
- Broos, P. S., Townsley, L. K., Getman, K., & Bauer, F. E. 2002, *ACIS Extract, An ACIS Point Source Extraction Package*, The Pennsylvania State University
- Cash, W. 1979, *ApJ*, 228, 939
- Chapman, S. C., Blain, A. W., Ivison, R. J., Smail, I. R. 2003a, *Nature*, 422, 695
- Chapman, S. C., et al. 2003b, *ApJ*, 585, 57
- Chapman, S. C., Windhorst, R., Odewahn, S., Yan, H., & Conselice, C. 2003c, *ApJ*, 599, 92
- Chapman, S. C., Smail, I., Windhorst, R., Muxlow, T., & Ivison, R. J. 2004a, *ApJ*, 611, 732
- Chapman, S. C., Scott, D., Windhorst, R. A., Frayer, D. T., Borys, C., Lewis, G. F., & Ivison, R. J. 2004b, *ApJ*, 606, 85
- Chapman, S. C., et al. 2005, *ApJ*, 622, 772
- Chartas, G., Brandt, W. N., Gallagher, S. C., & Garmire, G. P. 2002, *ApJ*, 579, 169
- Colbert, E. J. M., Heckman, T. M., Ptak, A. F., Strickland, D. K., & Weaver, K. A. 2004, *ApJ*, 602, 231
- Comastri, A., et al. 2002, *ApJ*, 571, 771
- Conselice, C. J., Chapman, S. C., & Windhorst, R. A. 2003, *ApJ*, 596, L5
- Cowie, L. L., Barger, A. J., & Kneib, J.-P. 2002, *AJ*, 123, 2197
- Cowie, L. L., Barger, A. J., Fomalont, E. B., & Capak, P. 2004, *ApJ*, 603, L69
- Croom, S. M., Smith, R. J., Boyle, B. J., Shanks, T., Miller, L., Outram, P. J., & Loaring, N. S. 2004, *MNRAS*, 349, 1397
- Deluit, S., & Courvoisier, T. J.-L. 2003, *A&A*, 399, 77
- Di Matteo, T., Springel, V., & Hernquist, L. 2005, *Nature*, 433, 604
- Eales, S., Lilly, S., Gear, W., Dunne, L., Bond, J. R., Hammer, F., Le Fèvre, O., & Crampton, D. 1999, *ApJ*, 515, 518
- Egami, E., et al. 2004, *ApJS*, 154, 130
- Elvis, M., et al. 1994, *ApJS*, 95, 1
- Erb, D. K., Shapley, A. E., Steidel, C. C., Pettini, M., Adelberger, K. L., Hunt, M. P., Moorwood, A. F. M., & Cuby, J. 2003, *ApJ*, 591, 101
- Fabian, A. C., Barcons, X., Almaini, O., & Iwasawa, K. 1998, *MNRAS*, 297, L11
- Fabian, A. C. 1999, *MNRAS*, 308, L39
- Fabian, A. C., et al. 2000, *MNRAS*, 315, L8
- Fabian, A. C., Sanders, J. S., Crawford, C. S., & Ettori, S. 2003, *MNRAS*, 341, 729
- Farrah, D., Afonso, J., Efstathiou, A., Rowan-Robinson, M., Fox, M., & Clements, D. 2003, *MNRAS*, 343, 585
- Fiore, F., et al. 2003, *A&A*, 409, 79
- Franceschini, A., Bassani, L., Cappi, M., Granato, G. L., Malaguti, G., Palazzi, E., & Persic, M. 2000, *A&A*, 353, 910



- Franceschini, A., et al. 2003, *MNRAS*, 343, 1181
- Frayer, D. T., Ivison, R. J., Scoville, N. Z., Yun, M., Evans, A. S., Smail, I., Blain, A. W., & Kneib, J.-P. 1998, *ApJ*, 506, L7
- Frayer, D. T. et al. 1999, *ApJ*, 514, L13
- Gallagher, S. C., Brandt, W. N., Chartas, G., & Garmire, G. P. 2002, *ApJ*, 567, 37
- Gehrels, N. 1986, *ApJ*, 303, 336
- Genzel, R., et al. 1998, *ApJ*, 498, 579
- Genzel, R., & Cesarsky, C. J. 2000, *ARA&A*, 38, 761
- Genzel, R., Baker, A. J., Tacconi, L. J., Lutz, D., Cox, P., Guillotheau, S., & Omont, A. 2003, *ApJ*, 584, 633
- George, I. M., Turner, T. J., Yaqoob, T., Netzer, H., Laor, A., Mushotzky, R. F., Nandra, K., & Takahashi, T. 2000, *ApJ*, 531, 52
- Gilfanov, M., Grimm, H.-J., & Sunyaev, R. 2004, *MNRAS*, 347, L57
- Granato, G. L., Silva, L., Danese, L., De Zotti, G., & Bressan, A. 2004a, Multiwavelength AGN surveys, Proceedings of the 8–12 December 2003 Conference, Cozumel, Mexico, eds. R. Mujica & R. Maiolino, Singapore: World Scientific, p.379
- Granato, G. L., De Zotti, G., Silva, L., Bressan, A., & Danese, L. 2004b, *ApJ*, 600, 580
- Greve, T. R., et al. 2005, *MNRAS*, in press (astro-ph/0503055)
- Grimm, H.-J., Gilfanov, M., & Sunyaev, R. 2003, *MNRAS*, 339, 793
- Haas, M., et al. 2003, *A&A*, 402, 87
- Helou, G., Soifer, B. T., & Rowan-Robinson, M. 1985, *ApJ*, 298, L7
- Hopkins, P. F., Hernquist, L., Martini, P., Cox, T. J., Robertson, B., Di Matteo, T., & Springel, V. 2005, *ApJ*, in press (astro-ph/0502241)
- Hornschemeier, A. E., et al. 2000, *ApJ*, 541, 49
- Hughes, D. H., Dunlop, J. S., & Rawlings, S. 1997, *MNRAS*, 289, 766
- Hughes, D. H., et al. 1998, *Nature*, 394, 241
- Isaak, K. G., Priddey, R. S., McMahon, R. G., Omont, A., Peroux, C., Sharp, R. G., & Withington, S. 2002, *MNRAS*, 329, 149
- Ivison, R. J., et al. 2002, *MNRAS*, 337, 1
- Ivison, R. J., Smail, I., Barger, A. J., Kneib, J.-P., Blain, A. W., Owen, F. N., Kerr, T. H., & Cowie, L. L. 2000, *MNRAS*, 315, 209
- Ivison, R. J., Smail, I., Le Borgne, J.-F., Blain, A. W., Kneib, J.-P., Bezecourt, J., Kerr, T. H., & Davies, J. K. 1998, *MNRAS*, 298, 583
- Ivison, R. J., et al. 2004, *ApJS*, 154, 124
- Iwasawa, K. 2001, *AIP Conf. Proc.* 599: X-ray Astronomy: Stellar Endpoints, AGN, and the Diffuse X-ray Background, 599, 169
- Iwasawa, K., Fabian, A. C., & Etori, S. 2001, *MNRAS*, 321, L15
- Iwasawa, K., Sanders, D. B., Evans, A. S., Trentham, N., Miniutti, G., & Spoon, H. W. W. 2005a, *MNRAS*, 357, 565
- Iwasawa, K., Crawford, C. S., Fabian, A. C., Cutri, R. M., & Wilman, R. J. 2005b, *MNRAS*, in press (astro-ph/0506305)
- Kaspi, S., et al. 2002, *ApJ*, 574, 643
- Kawakatu, N., Umemura, M., & Mori, M. 2003, *ApJ*, 583, 85
- Kim, D.-W., Fabbiano, G., & Trinchieri, G. 1992a, *ApJS*, 80, 645
- Kim, D.-W., Fabbiano, G., & Trinchieri, G. 1992b, *ApJ*, 393, 134
- King, A. 2003, *ApJ*, 596, L27
- Ledlow, M. J., Smail, I., Owen, F. N., Keel, W. C., Ivison, R. J., & Morrison, G. E. 2002, *ApJ*, 577, L79
- Lehmer, B. D., et al. 2005, *AJ*, 129, 1
- Lilly, S. J., Eales, S. A., Gear, W. K. P., Hammer, F., Le Fèvre, O., Crampton, D., Bond, J. R., & Dunne, L. 1999, *ApJ*, 518, 641
- Lira, P., Ward, M. J., Zezas, A., Alonso-Herrero, A., & Ueno, S. 2002, *MNRAS*, 330, 259
- Lockman, F. J. 2004, *Soft X-ray Emission from Clusters of Galaxies and Related Phenomena*, 111
- Lutz, D., Veilleux, S., & Genzel, R. 1999, *ApJ*, 517, L13
- Lutz, D., Sturm, E., Genzel, R., Spoon, H. W. W., Moorwood, A. F. M., Netzer, H., & Sternberg, A. 2003, *A&A*, 409, 867
- Lutz, D., Valiante, E., Sturm, E., Genzel, R., Tacconi, L. J., Lehnert, M. D., Sternberg, A., & Baker, A. J. 2005, *ApJ*, in press (astro-ph/0504431)
- Mainieri, V., Bergeron, J., Hasinger, G., Lehmann, I., Rosati, P., Schmidt, M., Szokoly, G., & Della Ceca, R. 2002, *A&A*, 393, 425
- Mainieri, V., et al. 2005a, *MNRAS*, 356, 1571
- Mainieri, V., et al. 2005b, *A&A*, in press (astro-ph/0502542)
- Maiolino, R., Salvati, M., Bassani, L., Dadina, M., della Ceca, R., Matt, G., Risaliti, G., & Zamorani, G. 1998, *A&A*, 338, 781
- Malizia, A., Bassani, L., Stephen, J. B., Di Cocco, G., Fiore, F., & Dean, A. J. 2003, *ApJ*, 589, L17
- Matt, G., Brandt, W. N., & Fabian, A. C. 1996, *MNRAS*, 280, 823
- Matt, G., Fabian, A. C., Guainazzi, M., Iwasawa, K., Bassani, L., & Malaguti, G. 2000, *MNRAS*, 318, 173
- McLure, R. J., & Dunlop, J. S. 2004, *MNRAS*, 352, 1390
- Moran, E. C., Lehnert, M. D., & Helfand, D. J. 1999, *ApJ*, 526, 649
- Mulchaey, J. S., Koratkar, A., Ward, M. J., Wilson, A. S., Whittle, M., Antonucci, R. R. J., Kinney, A. L., & Hurt, T. 1994, *ApJ*, 436, 586
- Mushotzky, R. F., Done, C., & Pounds, K. A. 1993, *ARA&A*, 31, 717
- Nandra, K. & Pounds, K. A. 1994, *MNRAS*, 268, 405
- Neri, R., et al. 2003, *ApJ*, 597, L113
- Ogle, P. M., Brookings, T., Canizares, C. R., Lee, J. C., & Marshall, H. L. 2003, *A&A*, 402, 849
- Nousek, J. A. & Shue, D. R. 1989, *ApJ*, 342, 1207
- Page, M. J., Stevens, J. A., Mittaz, J. P. D., & Carrera, F. J. 2001, *Science*, 294, 2516
- Page, M. J., Stevens, J. A., Ivison, R. J., & Carrera, F. J. 2004, *ApJ*, 611, L85
- Paolillo, M., Schreier, E. J., Giacconi, R., Koekemoer, A. M., & Grogin, N. A. 2004, *ApJ*, 611, 93
- Persic, M., Rephaeli, Y., Braito, V., Cappi, M., Della Ceca, R., Franceschini, A., & Gruber, D. E. 2004, *A&A*, 419, 849
- Pope, A., Borys, C., Scott, D., Conelice, C., Dickinson, M., & Mobasher, B. 2005, *MNRAS*, 358, 149
- Ptak, A., Serlemitsos, P., Yaqoob, T., & Mushotzky, R. 1999, *ApJS*, 120, 179
- Ranalli, P., Comastri, A., & Setti, G. 2003, *A&A*, 399, 39
- Richards, E. A. 2000, *ApJ*, 533, 611
- Rigopoulou, D., Spoon, H. W. W., Genzel, R., Lutz, D., Moorwood, A. F. M., & Tran, Q. D. 1999, *AJ*, 118, 2625
- Risaliti, G., Maiolino, R., & Salvati, M. 1999, *ApJ*, 522, 157
- Risaliti, G., Gilli, R., Maiolino, R., & Salvati, M. 2000, *A&A*, 357, 13
- Risaliti, G. 2002, *A&A*, 386, 379
- Salvati, M., & Maiolino, R. 2000, Large Scale Structure in the X-ray Universe, Proceedings of the 20-22 September 1999 Workshop, Santorini, Greece, eds. Plionis, M. & Georgantopoulos, I., Atlantis Sciences, Paris, France, p.277
- Sanders, D. B., & Mirabel, I. F. 1996, *ARA&A*, 34, 749
- Sanders, D. B., Mazzarella, J. M., Kim, D.-C., Surace, J. A., & Soifer, B. T. 2003, *AJ*, 126, 1607
- Scott, S., et al. 2002, *MNRAS*, 331, 817
- Severgnini, P., et al. 2000, *A&A*, 360, 457
- Severgnini, P., et al. 2005, *A&A*, 431, 87
- Shapley, A., Fabbiano, G., & Eskridge, P. B. 2001, *ApJS*, 137, 139
- Silk, J. & Rees, M. J. 1998, *A&A*, 331, L1
- Simpson, C., Dunlop, J. S., Eales, S. A., Ivison, R. J., Scott, S. E., Lilly, S. J., & Webb, T. M. A. 2004, *MNRAS*, 353, 179
- Smail, I., Ivison, R. J., & Blain, A. W. 1997, *ApJ*, 490, L5
- Smail, I., Ivison, R. J., Blain, A. W., & Kneib, J.-P. 2002, *MNRAS*, 331, 495
- Smail, I., Chapman, S. C., Ivison, R. J., Blain, A. W., Takata, T., Heckman, T. M., Dunlop, J. S., & Sekiguchi, K. 2003, *MNRAS*, 342, 1185
- Smail, I., Chapman, S. C., Blain, A. W., & Ivison, R. J. 2004, *ApJ*, 616, 71
- Smith, D. A., & Done, C. 1996, *MNRAS*, 280, 355
- Spoon, H. W. W., Koornneef, J., Moorwood, A. F. M., Lutz, D., & Tielens, A. G. G. M. 2000, *A&A*, 357, 898
- Springel, V., Di Matteo, T., & Hernquist, L. 2005, *MNRAS*, in press (astro-ph/0411108)
- Stark, A. A., Gammie, C. F., Wilson, R. W., Bally, J., Linke, R. A., Heiles, C., & Hurwitz, M. 1992, *ApJS*, 79, 77
- Steidel, C. C., Shapley, A. E., Pettini, M., Adelberger, K. L., Erb, D. K., Reddy, N. A., & Hunt, M. P. 2004, *ApJ*, 604, 534
- Stevens, J. A., et al. 2003, *Nature*, 425, 264
- Stevens, J. A., Page, M. J., Ivison, R. J., Smail, I., & Carrera, F. J. 2004, *ApJ*, 604, L17
- Sturm, E., Lutz, D., Verma, A., Netzer, H., Sternberg, A., Moorwood, A. F. M., Oliva, E., & Genzel, R. 2002, *A&A*, 393, 821
- Swinbank, A. M., Smail, I., Chapman, S. C., Blain, A. W., Ivison, R. J., & Keel, W. C. 2004, *ApJ*, 617, 64
- Swinbank, A. M., et al. 2005, *MNRAS*, in press (astro-ph/0502096)
- Szokoly, G. P., et al. 2004, *ApJS*, 155, 271
- Tran, Q. D., et al. 2001, *ApJ*, 552, 527
- Treister, E., et al. 2004, *ApJ*, 616, 123
- Turner, T. J., George, I. M., Nandra, K., & Mushotzky, R. F. 1997a, *ApJ*, 488, 164
- Turner, T. J., George, I. M., Nandra, K., & Mushotzky, R. F. 1997b, *ApJS*, 113, 23
- Verma, A., Rowan-Robinson, M., McMahon, R., & Andreas Efstathiou, A. E. 2002, *MNRAS*, 335, 574
- Vernet, J. & Cimatti, A. 2001, *A&A*, 380, 409
- IGNALI, C., Brandt, W. N., Fan, X., Gunn, J. E., Kaspi, S., Schneider, D. P., & Strauss, M. A. 2001, *AJ*, 122, 2143
- Wang, W.-H., Cowie, L. L., & Barger, A. J. 2004, *ApJ*, 613, 655
- Waskett, T. J., et al. 2003, *MNRAS*, 341, 1217
- Webb, T. M. A., et al. 2003a, *ApJ*, 587, 41
- Webb, T. M. A., Lilly, S. J., Clements, D. L., Eales, S., Yun, M., Brodwin, M., Dunne, L., & Gear, W. K. 2003b, *ApJ*, 597, 680
- Williams, R. E., et al. 1996, *AJ*, 112, 1335
- Wilman, R. J., Fabian, A. C., Crawford, C. S., & Cutri, R. M. 2003, *MNRAS*, 338, L19
- Yun, M. S., Reddy, N. A., & Condon, J. J. 2001, *ApJ*, 554, 803

TABLE 1. BASIC PROPERTIES OF THE SCUBA GALAXIES

| SCUBA Galaxy Properties |                   |                        | $z^a$ | Radio<br>$L_{1.4 \text{ GHz}}^b$ | Far-IR<br>$L_{\text{FIR}}^c$ | X-ray<br>ID <sup>d</sup> | X-ray             |                   | Band<br>Ratio <sup>e</sup>             | Effective<br>$\Gamma^e$                 | X-ray Source Properties |                         |                    |
|-------------------------|-------------------|------------------------|-------|----------------------------------|------------------------------|--------------------------|-------------------|-------------------|--|---|-------------------------|-------------------------|--------------------|
| $\alpha_{2000}^a$       | $\delta_{2000}^a$ | $S_{850\mu\text{m}}^a$ |       |                                  |                              |                          | $\alpha_{2000}^d$ | $\delta_{2000}^d$ |  |   | $f_{0.5-8\text{keV}}^f$ | $L_{0.5-8\text{keV}}^g$ | Class <sup>h</sup> |
| 12 35 49.44             | +62 15 36.8       | 8.3±2.5                | 2.203 | 24.38                            | 12.72                        | 35                       | 12 35 49.44       | +62 15 36.9       | 1.64 <sup>+0.67</sup> <sub>-0.50</sub> | 0.38 <sup>+0.33</sup> <sub>-0.31</sub>  | 1.34                    | 43.6                    | AGN                |
| 12 35 53.26             | +62 13 37.7       | 8.8±2.1                | 2.098 | 24.22                            | 12.56                        | ...                      | ...               | ...               | ...                                    | ...                                     | <0.19                   | <42.7                   | S/Burst?           |
| 12 35 55.14             | +62 09 01.7       | 5.4±1.9                | 1.875 | 24.67                            | 13.01                        | 44                       | 12 35 55.13       | +62 09 01.7       | 1.53 <sup>+0.27</sup> <sub>-0.24</sub> | 0.44 <sup>+0.15</sup> <sub>-0.15</sub>  | 11.25                   | 44.4                    | AGN                |
| 12 36 00.15             | +62 10 47.2       | 7.9±2.4                | 2.002 | 24.52                            | 12.87                        | ...                      | ...               | ...               | ...                                    | ...                                     | <0.19                   | <42.7                   | S/Burst?           |
| 12 36 06.72             | +62 15 50.7       | 4.4±1.4                | 2.416 | 23.97                            | 12.31                        | 77                       | 12 36 06.70       | +62 15 50.7       | 0.25 <sup>+0.05</sup> <sub>-0.04</sub> | 2.17 <sup>+0.32</sup> <sub>-0.29</sub>  | 1.69                    | 43.8                    | AGN                |
| 12 36 06.85             | +62 10 21.4       | 11.6±3.5               | 2.509 | 24.50                            | 12.84                        | 79                       | 12 36 06.84       | +62 10 21.4       | >2.18                                  | <0.12                                   | 0.74                    | 43.5                    | AGN                |
| 12 36 16.15             | +62 15 13.7       | 5.8±1.1                | 2.578 | 24.39                            | 12.73                        | 109                      | 12 36 16.11       | +62 15 13.7       | 0.85 <sup>+0.20</sup> <sub>-0.18</sub> | 0.97 <sup>+0.21</sup> <sub>-0.19</sub>  | 1.02                    | 43.7                    | AGN                |
| 12 36 18.33             | +62 15 50.5       | 7.3±1.1                | 1.865 | 24.52                            | 12.86                        | SUPP                     | 12 36 18.40       | +62 15 51.2       | ...                                    | 1.40                                    | 0.18                    | 42.6                    | S/Burst?           |
| 12 36 21.27             | +62 17 08.4       | 7.8±1.9                | 1.998 | 24.58                            | 12.92                        | ...                      | ...               | ...               | ...                                    | ...                                     | <0.11                   | <42.5                   | S/Burst?           |
| 12 36 22.65             | +62 16 29.7       | 7.7±1.3                | 2.466 | 24.46                            | 12.81                        | 135                      | 12 36 22.66       | +62 16 29.8       | >4.39                                  | <-0.50                                  | 1.02                    | 43.6                    | AGN                |
| 12 36 29.13             | +62 10 45.8       | 5.0±1.3                | 1.013 | 23.63                            | 11.97                        | 158                      | 12 36 29.11       | +62 10 45.9       | 2.05 <sup>+0.38</sup> <sub>-0.33</sub> | 0.18 <sup>+0.16</sup> <sub>-0.15</sub>  | 2.31                    | 43.1                    | AGN                |
| 12 36 32.61             | +62 08 00.1       | 4.9±1.2                | 1.993 | 24.36                            | 12.70                        | 171                      | 12 36 32.59       | +62 07 59.8       | 2.37 <sup>+0.68</sup> <sub>-0.53</sub> | 0.05 <sup>+0.23</sup> <sub>-0.22</sub>  | 1.83                    | 43.7                    | AGN                |
| 12 36 34.51             | +62 12 41.0       | 5.1±1.6                | 1.219 | 24.27                            | 12.61                        | 182                      | 12 36 34.50       | +62 12 41.2       | <0.41                                  | >1.63                                   | 0.29                    | 42.4                    | S/Burst?           |
| 12 36 35.59             | +62 14 24.1       | 4.7±1.3                | 2.005 | 24.35                            | 12.69                        | 190                      | 12 36 35.58       | +62 14 24.1       | 1.90 <sup>+0.30</sup> <sub>-0.27</sub> | 0.25 <sup>+0.14</sup> <sub>-0.13</sub>  | 2.52                    | 43.8                    | AGN (V)            |
| 12 36 36.75             | +62 11 56.1       | 7.0±2.1                | 0.555 | 22.70                            | 11.04                        | 194                      | 12 36 36.75       | +62 11 56.0       | 0.31 <sup>+0.03</sup> <sub>-0.03</sub> | 1.87 <sup>+0.09</sup> <sub>-0.09</sub>  | 3.77                    | 42.7                    | AGN (V)            |
| 12 37 07.21             | +62 14 08.1       | 4.7±1.5                | 2.484 | 24.27                            | 12.62                        | 347                      | 12 37 07.20       | +62 14 07.9       | 1.62 <sup>+0.48</sup> <sub>-0.39</sub> | 0.39 <sup>+0.25</sup> <sub>-0.23</sub>  | 0.98                    | 43.6                    | AGN                |
| 12 37 11.98             | +62 13 25.7       | 4.2±1.4                | 1.992 | 24.13                            | 12.48                        | 368                      | 12 37 12.04       | +62 13 25.7       | >4.11                                  | <-0.44                                  | 0.92                    | 43.4                    | AGN                |
| 12 37 12.05             | +62 12 12.3       | 8.0±1.8                | 2.914 | 24.10                            | 12.44                        | 369                      | 12 37 12.09       | +62 12 11.3       | 2.00 <sup>+1.45</sup> <sub>-0.88</sub> | 0.20 <sup>+0.52</sup> <sub>-0.49</sub>  | 0.38                    | 43.4                    | AGN                |
| 12 37 16.01             | +62 03 23.3       | 5.3±1.7                | 2.037 | 24.46                            | 12.80                        | 385                      | 12 37 16.04       | +62 03 23.7       | 0.42 <sup>+0.09</sup> <sub>-0.08</sub> | 1.61 <sup>+0.20</sup> <sub>-0.17</sub>  | 7.36                    | 44.3                    | AGN (V)            |
| 12 37 21.87             | +62 10 35.3       | 12.0±3.9               | 0.979 | 23.29                            | 11.63                        | 405                      | 12 37 21.86       | +62 10 35.8       | 5.07 <sup>+2.43</sup> <sub>-1.52</sub> | -0.63 <sup>+0.32</sup> <sub>-0.35</sub> | 2.11                    | 43.1                    | AGN (V)            |

<sup>a</sup> SCUBA galaxy properties, taken from Chapman et al. (2005). Submm flux density is in units of mJy.

<sup>b</sup> Rest-frame 1.4 GHz luminosity density in logarithmic units of  $\text{W Hz}^{-1}$ . Calculated following equation 2 in Alexander et al. (2003b) for  $\alpha = 0.8$  (the average spectral index for star-forming galaxies; e.g., Yun, Reddy, & Condon 2001) using the radio flux density from Chapman et al. (2005).

<sup>c</sup> Rest-frame far-IR ( $\lambda = 40\text{--}120 \mu\text{m}$ ) luminosity in logarithmic units of solar luminosities. Calculated from the rest-frame 1.4 GHz luminosity under the assumption of the radio to far-IR correlation with  $q = 2.35$  (e.g., Helou, Soifer, & Rowan-Robinson 1985).

<sup>d</sup> X-ray source identification number and X-ray source co-ordinates; taken from Alexander et al. (2003a). ‘‘SUPP’’ refers to a source detected in the complete supplementary *Chandra* catalog; see Alexander et al. (2003b), §3.2 and §3.4.2 of Alexander et al. (2003a).

<sup>e</sup> Ratio of the count rates in the 2.0–8.0 keV and 0.5–2.0 keV bands, and the effective photon index in the 0.5–8.0 keV band (calculated from the band ratio); taken from Alexander et al. (2003a).  $\Gamma = 1.4$  has been adopted for sources with poorly defined band ratios.

<sup>f</sup> Full-band flux uncorrected for Galactic or intrinsic absorption, in units of  $10^{-15} \text{ erg cm}^{-2} \text{ s}^{-1}$ . Taken from Alexander et al. (2003a,b). Upper limits are calculated following §3.4.1 of Alexander et al. (2003a).

<sup>g</sup> Rest-frame 0.5–8.0 keV luminosities in logarithmic units of  $\text{erg s}^{-1}$ , calculated following equation 1 in Alexander et al. (2003b) for  $\Gamma = 1.8$ .

<sup>h</sup> Source classification based on X-ray properties; see §3.2. ‘‘AGN’’ indicates the X-ray emission is dominated by AGN activity, ‘‘(V)’’ indicates evidence for X-ray variability, and ‘‘S/Burst?’’ indicates that the X-ray emission is probably dominated by luminous star-formation activity.

TABLE 2. SPECTRAL FITS FOR THE AGN-CLASSIFIED SCUBA GALAXIES

| $\alpha_{2000}^a$ | X-ray $\delta_{2000}^a$ | Rest-Frame Energies <sup>b</sup> | X-ray Counts <sup>c</sup> | X-ray Spectral Fits                     |   | $N_{\text{H}}^e$ | X-ray Luminosities     |                        |                              |                             |
|-------------------|-------------------------|----------------------------------|---------------------------|---|---|------------------|------------------------|------------------------|------------------------------|-----------------------------|
|                   |                         |                                  |                           | $\Gamma(2-10 \text{ keV})^d$            | $\Gamma(5-20 \text{ keV})^d$            |                  | $L_{2-10\text{keV}}^f$ | $L_{5-20\text{keV}}^f$ | $L_{0.5-8\text{keV,corr}}^g$ | $L_{0.5-8\text{keV,pow}}^h$ |
| 12 35 49.44       | +62 15 36.9             | 1.6–32.0                         | 117                       | +0.71 <sup>+0.83</sup> <sub>-0.88</sub> | -0.30 <sup>+0.52</sup> <sub>-0.81</sub> | 24.0             | 43.0                   | 43.6                   | 44.0                         | 44.2                        |
| 12 35 55.13       | +62 09 01.7             | 1.4–28.8                         | 189                       | +0.10 <sup>+0.37</sup> <sub>-0.38</sub> | +1.29 <sup>+0.42</sup> <sub>-0.41</sub> | 23.0             | 44.0                   | 44.3                   | 44.4                         | 44.5                        |
| 12 36 06.70       | +62 15 50.7             | 1.7–34.2                         | 347                       | +1.89 <sup>+0.27</sup> <sub>-0.27</sub> | +2.07 <sup>+0.37</sup> <sub>-0.38</sub> | 20.0             | 43.7                   | 43.7                   | 43.8                         | 43.9                        |
| 12 36 06.84       | +62 10 21.4             | 1.8–35.1                         | 55                        | ...                                     | +0.10 <sup>+0.67</sup> <sub>-0.52</sub> | 24.0             | <42.8                  | 43.4                   | 43.7                         | 43.9                        |
| 12 36 16.11       | +62 15 13.7             | 1.8–35.8                         | 108                       | +0.37 <sup>+0.54</sup> <sub>-0.55</sub> | +1.34 <sup>+0.44</sup> <sub>-0.52</sub> | 23.0             | 43.4                   | 43.6                   | 43.7                         | 43.8                        |
| 12 36 22.66       | +62 16 29.8             | 1.7–34.7                         | 71                        | ...                                     | -0.76 <sup>+0.61</sup> <sub>-0.69</sub> | 24.2             | <42.7                  | 43.6                   | 44.0                         | 44.3                        |
| 12 36 29.11       | +62 10 45.9             | 1.0–20.1                         | 178                       | +0.15 <sup>+0.29</sup> <sub>-0.29</sub> | +1.54 <sup>+0.74</sup> <sub>-0.64</sub> | 23.0             | 42.8                   | 43.0                   | 43.2                         | 43.2                        |
| 12 36 32.59       | +62 07 59.8             | 1.5–29.9                         | 136                       | -0.05 <sup>+0.59</sup> <sub>-0.62</sub> | +0.22 <sup>+0.51</sup> <sub>-0.53</sub> | 23.8             | 43.1                   | 43.6                   | 43.9                         | 44.0                        |
| 12 36 35.58       | +62 14 24.1             | 1.5–30.1                         | 217                       | -0.07 <sup>+0.40</sup> <sub>-0.40</sub> | +0.63 <sup>+0.33</sup> <sub>-0.33</sub> | 23.7             | 43.3                   | 43.7                   | 44.0                         | 44.1                        |
| 12 36 36.75       | +62 11 56.0             | 0.8–15.6                         | 650                       | +1.82 <sup>+0.22</sup> <sub>-0.21</sub> | ...                                     | 20.0             | 42.4                   | ...                    | 42.7                         | 42.7                        |
| 12 37 07.20       | +62 14 07.9             | 1.7–34.8                         | 78                        | -0.52 <sup>+0.75</sup> <sub>-0.81</sub> | +0.74 <sup>+0.49</sup> <sub>-0.49</sub> | 23.5             | 43.2                   | 43.6                   | 43.8                         | 43.9                        |
| 12 37 12.04       | +62 13 25.7             | 1.5–29.9                         | 52                        | ...                                     | +0.04 <sup>+0.67</sup> <sub>-0.71</sub> | 24.0             | <42.7                  | 43.3                   | 43.6                         | 43.8                        |
| 12 37 12.09       | +62 12 11.3             | 2.0–39.1                         | 32                        | +1.34 <sup>+1.49</sup> <sub>-1.81</sub> | +0.23 <sup>+1.09</sup> <sub>-1.30</sub> | 23.8             | 42.6                   | 43.2                   | 43.4                         | 43.6                        |
| 12 37 16.04       | +62 03 23.7             | 1.5–30.4                         | 278                       | +1.14 <sup>+0.29</sup> <sub>-0.29</sub> | +1.63 <sup>+0.57</sup> <sub>-0.37</sub> | 22.5             | 44.1                   | 44.2                   | 44.3                         | 44.4                        |
| 12 37 21.86       | +62 10 35.8             | 1.0–19.8                         | 120                       | -0.63 <sup>+0.43</sup> <sub>-0.24</sub> | +0.79 <sup>+0.69</sup> <sub>-0.68</sub> | 23.5             | 42.7                   | 43.1                   | 43.3                         | 43.4                        |

<sup>a</sup> X-ray source position, taken from Table 1.<sup>b</sup> Corresponding rest-frame energy (keV) for the observed 0.5–10 keV band.<sup>c</sup> Total number of 0.5–10 keV counts used in the X-ray spectral analyses.<sup>d</sup> Best-fit photon index for a simple power-law model (with Galactic absorption) in the indicated rest-frame energy bands; the uncertainties refer to the 90% confidence level (for one interesting parameter).<sup>e</sup> Estimated X-ray absorbing column density in logarithmic units of  $\text{cm}^{-2}$ . See §3 for justification and column density analyses.<sup>f</sup> Rest-frame X-ray luminosity, determined directly from XSPEC using the best-fit photon indices. This has not been corrected for absorption.<sup>g</sup> Rest-frame 0.5–8.0 keV luminosity in logarithmic units of  $\text{erg s}^{-1}$ , determined from the rest-frame 5–20 keV luminosity and corrected for the estimated X-ray absorbing column density using our adopted AGN model; see §3.5.<sup>h</sup> Rest-frame 0.5–8.0 keV luminosity in logarithmic units of  $\text{erg s}^{-1}$ , determined from the rest-frame 5–20 keV luminosity and corrected for the estimated X-ray absorbing column density using a simple absorbed power-law model; see §3.5.